Brijesh Upadhaya

Design of Torque Exciter for Induction Machine

School of Electrical Engineering

Thesis submitted for examination for the degree of Master of Science in Technology.

Espoo 07.04.2014

Thesis supervisor:

Prof. Antero Arkkio

Thesis advisor:

Prof. Antero Arkkio

Aalto University
School of Electrical
Engineering

AALTO UNIVERSITY
SCHOOL OF ELECTRICAL ENGINEERING

ABSTRACT OF THE
MASTER'S THESIS

Author: Brijesh Upadhaya

Title: Design of Torque Exciter for Induction Machine

Date: 07.04.2014 Language: English Number of pages:10+49

Department of Electrical Engineering & Automation

Professorship: Electromechanics Code: S-17

Supervisor: Prof. Antero Arkkio

Advisor: Prof. Antero Arkkio

Three phase induction machines are becoming more popular and are also being used as variable speed drives. An induction machine driving a load represents a torsional system. The analysis of any torsional system without active damper is somehow based on conventional method i.e. including shaft stiffness and viscous damping provided by the material. This conventional method might lead to somehow highly compromised results. The involvement of induction machine complicates the approach by contributing to both stiffness and damping in the system. So, in-order to verify the contribution from the electromagnetic system in overall torsion dynamics of the drive train, a thorough study on torque exciter has been carried out in this master's thesis work. A new type of excitation system has been proposed on the basis of studied material. A careful investigation on stability of the proposed excitation system has also been performed followed by laboratory set-up and testing. Finally, measurements were carried out to verify the electromagnetic system's contribution toward both stiffness and damping. A brief comparison between simulation results with measurement result has been presented.

Keywords: Induction machine, Torsional dynamics, Torque exciter

Acknowledgments

I would like to thank my immediate supervisor and advisor Prof. Antero Arkkio for providing me with useful guidance and feedback throughout my work, and also trusting me for this work. A big thank to Research Foundation of Helsinki University of Technology for providing with a scholarship for this research work. I would also like to thank Ari Haavisto, operating engineer at Department of Electrical Engineering and Automation, from bottom of my heart for his continuous support to build the laboratory set-up for measurement. I express gratitude to my colleagues Antti Lehikoinen and Bishal Silwal for their feedbacks and useful discussions on my work. Also, I would like to sincerely thank D.Sc. Paavo Rasilo and Javier Martinez for providing ideas related to signal processing. A special thanks to Matti Mustonen from ABB drives, for his support in frequency converter control algorithms. Lastly, it was indeed a great opportunity to be part of electro-mechanics research group in Aalto University.

I would like to dedicate this work to my mother Radha Upadhaya for her continuous encouragement for a better performance.

Otaniemi, 07.04.2014

Brijesh Upadhaya

Contents

List of Figures

List of Tables

Symbols and abbreviations

Symbols

α_i	Real part of Eigenvalue
δ	Torsion angle
Δ	Small change
ζ	Damping ratio
Θ	Combined rotation angle
θ	Rotation angle
ϑ	Position angle of the reference frame
λ_i	Eigenvalue
ρ	Specific density
σ	Total leakage factor
τ_e	Electro-magnetic Torque
ψ	Flux-linkage
$\underline{\psi}_\mathrm{s}$	Stator flux-linkage space vector
$\underline{\psi}_\mathrm{r}$	Rotor flux-linkage space vector
ψ_sx, ψ_sy	Real and imaginary component of stator flux-linkage space vector
ψ_rx, ψ_ry	Real and imaginary component of rotor flux-linkage space vector
ω_e	Angular velocity in electrical degrees
ω_i	Imaginary part of Eigenvalue
ω_k	Speed of rotating reference frame
ω_0	Steady-state angular velocity
ω_s	Synchronous speed
Ω	Combined angular speed and also used for representing ohm

A	Ampere
$\mathbf{A}$	Characteristic matrix of the system
$\mathbf{B}$	System input matrix
B	Mechanical friction constant
C	Damping constant
f	Frequency in Hertz
$\underline{i}_\mathrm{s}$	Stator current space vector
$\underline{i}_\mathrm{r}$	Rotor current space vector
i_sx, i_sy	Real and imaginary component of stator current space vector
i_rx, i_ry	Real and imaginary component of rotor current space vector
$\mathbf{I}$	Identity Matrix
j	Imaginary unit
J	Mass moment of inertia
$\mathbf{K}$	Matrix of torsional spring constant
K_s	Stator Coupling Factor
K_r	Rotor Coupling Factor
L_s	Stator Inductance
L_r	Rotor Inductance

L_{m}	Magnetizing Inductance
$L_{\mathrm{r}\sigma}$	Rotor Leakage Inductance
$L_{\mathrm{s}\sigma}$	Stator Leakage Inductance
L'_{s}	Stator Inductance: Transient
L'_{r}	Rotor Inductance: Transient
$\mathbf{M}$	Mass Matrix
$p, \boldsymbol{p}$	Number of pole pairs
R_{s}	Stator resistance
R_{r}	Rotor resistance
S	Slip
s	Laplace variable
T	Torque
T'_{s}	Transient time constant: Stator
T'_{r}	Transient time constant: Rotor
$\mathbf{u}$	Input vector
u	Voltage
u_{s}	Stator Voltage
$\underline{u}_{\mathrm{s}}$	Stator voltage space vector
$\underline{u}_{\mathrm{r}}$	Rotor voltage space vector
u_{sx}, u_{sy}	Real and imaginary component of stator current space vector
u_{rx}, u_{ry}	Real and imaginary component of rotor current space vector
V	Volts
$\mathbf{x}$	State vector
X_{s}	Stator Reactance
X'_{s}	Transient Reactance: Stator
X_{r}	Rotor Reactance
X'_{r}	Transient Reactance: Rotor
X_{m}	Magnetizing Reactance

Operators

$\dfrac{\mathrm{d}}{\mathrm{d}t}$	Derivative with respect to t
$\dfrac{\mathrm{d}^2}{\mathrm{d}t^2}$	Second derivative with respect to t
$[\ldots]^T$	Transpose of a matrix
$\mathrm{Im}\{\ldots\}$	Imaginary operator
$\mathrm{Re}\{\ldots\}$	Real operator
$\{\ldots\}^*$	Complex conjugate

Abbreviations

AC	Alternating current
CSI	Current Source Inverter
DC	Direct current
DFT	Discrete Fourier Transform
Eq.	Equation
FEA	Finite Element Analysis
FEM	Finite Element Method
Fig.	Figure
FFT	Fast Fourier Transform
FRF	Frequency Response Function
GPa	Gigapascal
Hz	Hertz
IEEE	Institute of Electrical and Electronics Engineers
kg	Kilogram
kW	kilowatt
Nm	Newton-meter
PM	Permanent Magnet
pp.	Pages
ppr	Pulse per revolution
PWM	Pulse Width Modulation
rad	Radian
RPM	Rotation Per Minute
SDF	Single Degree of Freedom
sec	Second
vol.,Vol.	Volume number
VSD	Variable speed drive
VFD	Variable Frequency Drive
VSI	Voltage Source Inverter

1 Introduction

1.1 Problem Statement

With the advancement in the control techniques and power converters, induction machine has been the main constituent in the industrial sector. Mainly used as variable speed drive (VSD), induction machine has taken lead share of the total power consumed among electrical machines in industrial sector. Induction machine's dominance in the industrial sector is mainly due to its ruggedness (cage type), usability in hazardous environment, economical, and mature control technique. So, ruggedness provides an obvious advantage over its old rival DC machine, which needed periodic maintenance on its commutator-brush section. Although of having ample of merits it has certain demerits as well which includes: low starting torque, high starting current, and torque pulsation. Especially high torque pulsation and poor starting are mainly in case of single phase induction machines. But single phase induction machines are used only for small power applications, where torque pulsation is not a big issue. In higher power application 3-phase induction machines are used due to constant power output (mechanical: shaft-output power), and relatively small toque pulsation.

The development of power diodes, thyristors, and IGBTs in early 90's enhanced researchers to put forward robust control algorithm for making use of rugged induction machine applicable in variable speed drives. Although of high complexity involved in power converters, various control techniques have emerged, viz. direct torque control (DTC), Scalar control (V/F control) and Vector control. Nowadays DTC and vector control techniques are mostly used due to their quality performance. Induction machines are non-linear, and non-linearity is essentially associated with the core material, typically an iron. Also, induction machines consist of an air-gap between stationary stator and movable rotor. The length of air-gap typically is less than 2 mm. Also, electro-mechanical energy conversion process takes place in the air-gap. The torque production is a result of interaction between stator flux and rotor current. The main forces are on the protruding component of stator and rotor core, commonly called teeth. However, a small percentage of the total force is confined to the windings, namely Lorentz force. The air-gap flux in the machine is non-sinusoidal and consist of harmonics due to non-linearity. The current however is sinusoidal, so taking these considerations we can study the behaviour of the air-gap torque. The electromagnetic torque of an induction machine can be expressed as

$$\tau_e = \frac{3}{2} p \mathrm{Im}\left\{\underline{\psi}_\mathrm{s}^* \underline{i}_\mathrm{s}\right\} \tag{1.1}$$

where, p is the pole pair number, $\underline{\psi}_\mathrm{s}$ is the stator flux-linkage space vector, and $\underline{i}_\mathrm{s}$ is the stator current space vector. We can further express stator current space vector and stator flux-linkage space vector as a sum of frequency components

$$\underline{i}_\mathrm{s} = \hat{i}_s e^{\mathrm{j}\omega_1 t} \tag{1.2}$$

$$\underline{\psi}_\mathrm{s} = \left(\hat{\psi}_1 e^{\mathrm{j}(\omega_1 t+\varphi_1)} + \hat{\psi}_5 e^{-\mathrm{j}(5\omega_1 t+\varphi_5)} + \hat{\psi}_7 e^{\mathrm{j}(7\omega_7 t+\varphi_7)} + \cdots\right) \tag{1.3}$$

Now substituting Eq. (1.2) and Eq. (1.3) in Eq. (1.1) we obtain

$$\tau_e = \frac{3\hat{i}_s}{2} p \mathrm{Im}\left\{\hat{\psi}_1 e^{-\mathrm{j}\varphi_1} + \hat{\psi}_5 e^{\mathrm{j}(6\omega_1 t+\varphi_5)} + \hat{\psi}_7 e^{-\mathrm{j}(6\omega_1 t+\varphi_7)} + \cdots\right\} \tag{1.4}$$

Clearly, the torque will comprise of pulsation at angular frequencies $6n\omega_1$, where $n = 1, 2, 3, \ldots$. The $6th$ harmonic is the resultant of $5th$ and $7th$ harmonic components, i.e., $5th$ being a negative sequence and rotating in the opposite direction with respect to the fundamental component while $7th$ being the positive sequence and rotating in the direction of the fundamental component. The resultant would then rotate in the direction of the fundamental with a speed $6\omega_1$. The fundamental component is responsible for the constant toque in the machine while harmonic components give rise to the oscillation or torque pulsation [1]. Although of small amplitude these harmonics can excite torsional resonance if they coincide with the mechanical natural frequency of the system. Also, if the damping is not enough then the vibration would amplify leading to catastrophic failure. Induction machines are still direct on line connected as compared to frequency converter fed. However, in case of converter supplied machine both voltage and current are distorted, demanding more complicated analysis. The harmonics in the air-gap torque are even more prominent.

Hence, above statement signify a need for careful investigation to be done in-order to avoid shaft fatigue and eventual failure of an induction machine while used as a VSD. Investigation here would mean calculation of torsional natural frequencies and possible excitation torques in the system. A torsional system must be able to avoid coincidence with the torsional natural frequencies within its operating speed. In case of VSD it may not be possible to avoid all the possible torsional natural frequency due to wide speed range of the drive system. This creates a need for thorough analysis to be done on shaft stresses and coupling torques [2]. Also, in such a case damping plays a vital role and must be studied. In addition to viscous damping, damping provided by electrical machine might be vital. Any change in the effective torsional stiffness and damping affects the natural frequency of the overall system; therefore study must be done to clarify this phenomenon. The latter study and experiment is mainly based on the study of torsional vibration in cage-induction machine and possible excitation system.

1.2 Objectives

The main objective of this work are

- To study previously done research on torsion excitation system and propose a suitable excitation system for 37 kW cage induction machine
- To build torsion excitation system for 37 kW cage induction machine for conducting the laboratory experiment, and validating the simulation result shown in Fig. 1.1

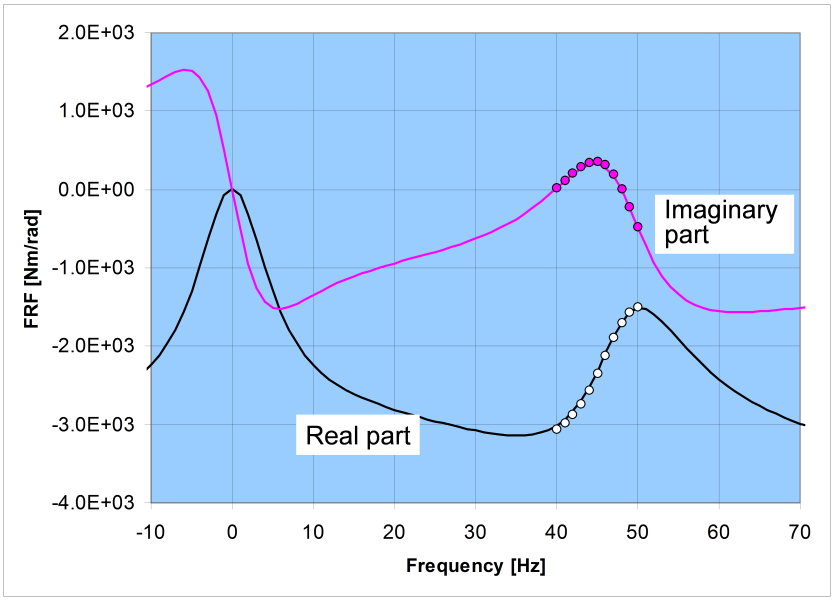

Figure 1.1: Impulse response from rotor position angle to torque

Fig. 1.1 is the simulation[1] result that represents impulse response of torsion angle to torque in frequency domain of a 37 kW cage-induction machine. The impulse has excited all the frequencies in the range –200 Hz to +200 Hz. But, the main study area lies within frequency range of 0 Hz –100 Hz where the possible operating range of induction machine lies.

The smooth lines are results from impulse response, while the dots represent simulation result from harmonic excitation at particular frequencies. The impulse response consists of both real and imaginary part, and to make a brief explanation on the simulation result we need to formulate an analytical model. However, the simple explanation would be the real part of the FRF corresponds to the electromagnetic spring constant, and the imaginary part corresponds to the damping provided by electromagnetic system. The most interesting result from this simulation is that the damping is negative in the frequency range of 40 Hz – 49 Hz. The electromagnetic system will try to feed power to the torsional vibration within the frequency range of 40 Hz – 49 Hz. However, the damping is positive in other frequency range (0 Hz–70 Hz), resulting in power extraction from the vibration. There might be some confusion arising due to term negative electromagnetic damping. The above statements are based upon reference taken for a motoring mode, where both the air-gap power and torque are taken to be positive. The Section 3 will clarify positive and negative damping conditions. Now, if the torsional natural frequency of the system lies within the frequency range of 40 Hz – 50 Hz, then the machine could be unstable. Validating the simulation result of Fig. 1.1 through measurement is the main goal of this master's thesis work.

[1]The simulation of Fig. 1.1 was performed by Prof. Antero Arkkio, Department of Electrical Engineering & Automation, Aalto University

1.3 Thesis Structure

The latter part of the study is divided into following chapters, viz.

Chapter 2 :Outlines some of the previously done research work in torsional excitation system.

Chapter 3 :Presents the set-up for proposed excitation system followed by the assumptions and mechanical model for analysis of torsional system. It follows the complete procedure for analysing the torsional system.

Chapter 4 :Presents the space-vector model of induction machine. On the basis of this model a small-signal model is formulated and further stability analysis of the proposed system is performed. Analytical model for both impulse response test and harmonic excitation is also formulated.

Chapter 5 :This chapter presents the complete layout of proposed excitation system and simulation results from the small-signal analysis. Then measurement results from the laboratory test are presented and briefly explained.

Chapter 6 :Compares the simulation result with the measurement result. Finally, concludes the work.

2 Previous Research

The research on torsional vibration started later as compared to lateral vibration. Unlike lateral vibration, torsional vibration is relatively difficult to distinguish because of no immediate symptoms. It is quite difficult to clarify the occurrence of torsional vibration just by looking at the rotating system (or shafts), because the vibration is superimposed on the steady rotational motion of the machine. But, in geared systems, clattering noise might be an indication of torsional vibration [3]. Gradually, rotating systems were subject to torsional oscillation which resulted into gear wear, key failures, and even broken shafts in long run. Researchers then devised methods to measure such phenomenon and finally to solutions for such problem. The present day torsion vibration measurement uses either optical encoder or laser based non-contact system (laser torsional vibro-meter) [4].

With the availability of mature measurement technology, much of the work are now carried out on torsional oscillations and method to lessen the effect of such vibration. Fred *et al.* [2] have made an analysis on torsional vibration in rotating machinery. The analysis consists of very much detail about the mathematical model of the torsional system. Similarly, Corbo and Malanoski [5] have provided a detail manual on practical design consideration against torsional vibration, also a very recent work from Holopainen *et al.* [6] have provided a brief outline on analysis of torsional vibration in rotating machines used as VFD. Hence, these manuals form the basis for this master thesis work as well.

2.1 Early Excitation Systems

One of the early excitation system proposed by J. P. Conniff *et al.* [7] makes use of a DC motor as a torsional exciter. The working principle of the excitation system was such that the armature winding of the machine was supplied by a DC source along with superimposed AC supply. The field supply was however kept constant. The DC source provided for the net torque for rotation and AC supply being responsible for torque pulsation, while the shaft of the motor was coupled to the test inertia load. The patent claims that the torque oscillation frequency could be varied smoothly in a wide range, simply by adjusting the frequency of superimposed AC component. Further development in the field of torsional exciter for rotating structure was then carried by Zobrist *et al.* [8], who proposed use of relatively simple mechanism for excitation. Also, to be mentioned, the paper claims suitability of the excitation system for any size and shape of the rotating structure. The experimental exciter included a rotary hydraulic actuator mounted directly on the test object's shaft.

After the year 1990 A.D. with AC machines dominance as a VSD, Drew *et al.* [9] proposed use of AC servo motor as a combined drive motor and torsional exciter. The torsional excitation system was especially for low power rotating machinery application. Some experiments were conducted to determine the torsional stiffness and damping level provided by the servo drive. Secondly, the same servo-drive was then used as a torsional exciter in another experiment, where a small single cylinder engine (with no gas forces) was used. Torque oscillations from the servo

drive were produced due to oscillatory (speed control) input signal fed to the servo amplifier. The oscillatory signal was generated by superimposing AC component on a DC voltage. This experiment was mainly focused on study related to second-order inertia variation while rotating the drive system [10].

2.2 Recent Excitation Systems

A much recent work involves that of Christof Sihler [11], who proposed a novel torsional exciter for a rotating system in high power application. The distinguishing feature from Sihler's work was that, the excitation system makes use of an electromagnetic excitation technique. The proposed excitation system was used for analysing torsional vibration in three phase flywheel generator at IPP (Max-Planck-Institut für Plasmaphysik). The exciter has been characterized of having no fixture to the test object's rotating shaft, because the torsional excitation was applied by means of stator winding of the electrical machine. Sihler's method was based on modulation of stator current so that the air-gap torque would then consist of harmonics leading to oscillation in the rotor speed. This was done by feeding the current controlled load by the generator. The control mechanism was done in such a way that the torsion excitation of desired amplitude and frequency could be introduced in the generator shaft assembly. The paper claims that the novel exciter could be suitable for on-site testing of large electrical machines due to portable and no external source requirement.

The copied layout from Sihler's [11] work is presented in Fig. 2.1. The torque measurement was done via coupling between flywheel and the generator shaft, as labelled in Fig. 2.1. The prime mover before the flywheel is not clearly visible, while the load is connected in the secondary of the step-down transformer. It is

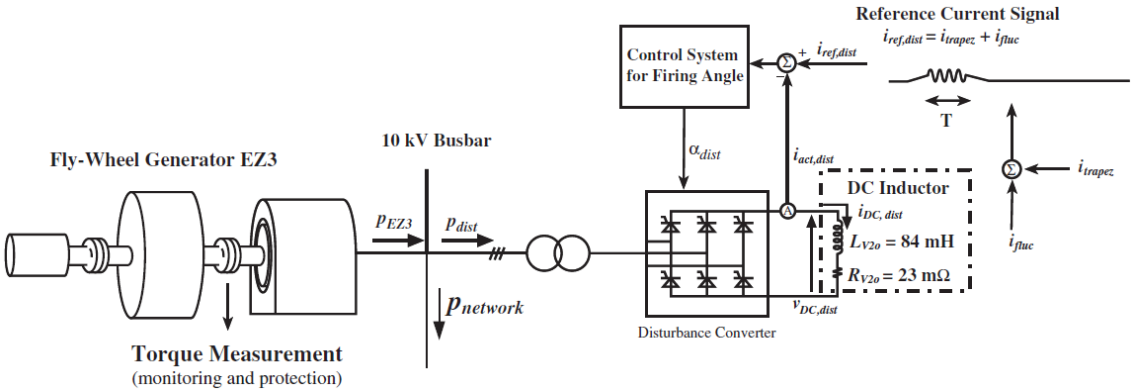

Figure 2.1: Experimental set-up [11]

evident from the layout that the load involves thyristor feeding RL load. The control mechanism has been done in such a way that the oscillatory current signal was provided to the firing circuit.

Further continuation of work on torsional excitation system includes that of Leong *et al.* [12]. The presented work from Leong *et al.* includes a novel method

which makes use of cogging torque as necessary excitation. The main purpose of the experiment was to determine the mechanical resonance of permanent magnet brush-less drive for torsional vibration analysis. The paper presents that the cogging torque produced due to slotting of the stator core in PM machine is of approximately sinusoidal in shape. This sinusoidally distributed cogging toque has been the main cause in circumferential vibration. It has been claimed that under open-circuit condition and at room temperature the amplitude of cogging torque waveform is essentially constant despite of change in speed. This is taken to be an obvious advantage, as it could constantly provide torsional excitation within the needed frequency range. The test set-up consists of a PM machine coupled to a servo drive, which essentially is a DC machine [12]. A copy of experimental set-up presented by Leong *et al.* is shown in Fig. 2.2.

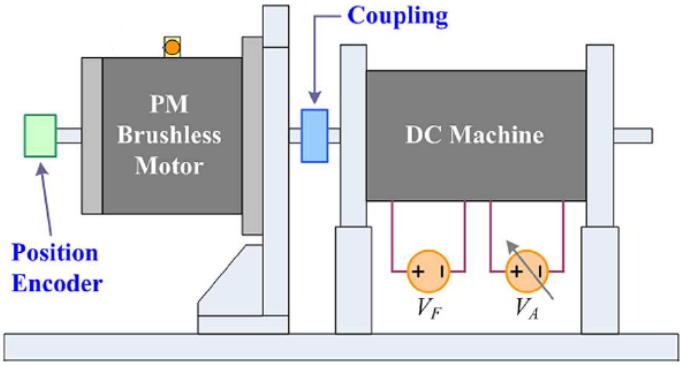

Figure 2.2: Experimental set-up [12]

2.3 Summary

The main essence from previously presented excitation systems underlies the fact that either electromagnetic excitation system could be one of the possible excitation systems or excitation from the load machine (which is simply coupled to the driving machine) could be possible. Also, the control parameter (which is the excitation amplitude and frequency) could be smoothly manipulated when electromagnetic excitation system is chosen. This seems controlling the air-gap torque would be the most useful way to produce the necessary excitation.

3 Mechanical Model

3.1 Proposed Excitation System

On the basis of the previously presented excitation system a new set-up has been proposed. The proposed excitation system here makes use of a three phase cage induction machine fed from a frequency converter as an exciter. The test object here is also a three phase, four pole 37 kW cage induction machine and the proposed exciter is a four pole 4 kW cage induction machine. The exciter machine will be supplied from the frequency converter. Frequency converter here is the source for production of harmonic air-gap torque, which essentially is transmitted to the drive shaft for possible excitation. The frequency converter will be accommodated with the necessary control algorithm for the production of harmonic air-gap torque. Exciter machine's rating will be determined in such a way that the mechanical natural frequency of the coupled system lies away from the test range (0 Hz – 100 Hz). Also, from the view point of needed excitation, the exciter machine's rating has been taken as 10% of the 37 kW machine. The rotor shaft of the exciter machine is coupled to the shaft of test machine via a flexible coupling as shown in Fig. 3.1.

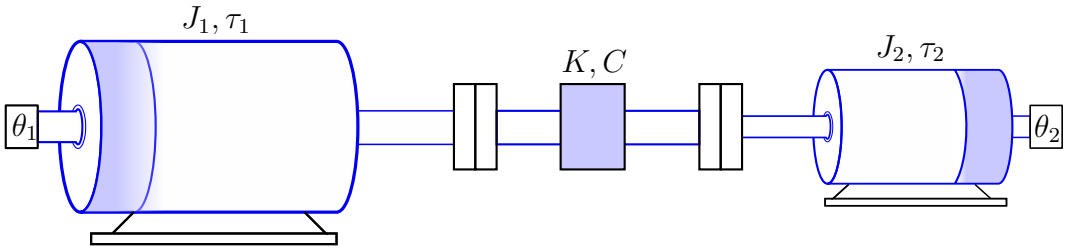

Figure 3.1: Proposed layout for torsion excitation

Fig. 3.1 represents one of the possible set-ups. J_1 and J_2 represent the mass moment of inertia of the rotors of the machines, τ_1 and τ_2 represent the external torque acting on the rotor, which essentially is the air-gap torque, θ_1 and θ_2 represent the position angle of the rotor shafts, C is the damping coefficient, and K represent the spring constant of the shaft-coupling arrangement. Both induction machines are run at no-load condition, while the exciter machine is fed via a frequency converter, and the test machine is supplied from grid. The function of smaller machine is only to produce necessary excitation torque, and in this experiment harmonic excitation at desired frequency range shown in Fig. 1.1.

3.2 Torsional Vibration in Two Mass System

The equation of motion for two mass system shown in Fig. 3.2 can be written as

$$J_1\frac{\mathrm{d}^2\theta_1}{\mathrm{d}t^2} + B_1\frac{\mathrm{d}\theta_1}{\mathrm{d}t} + C\frac{\mathrm{d}(\theta_1-\theta_2)}{\mathrm{d}t} + K(\theta_1-\theta_2) = T_1(t) \tag{3.1}$$

$$J_2\frac{\mathrm{d}^2\theta_2}{\mathrm{d}t^2} + B_2\frac{\mathrm{d}\theta_2}{\mathrm{d}t} + C\frac{\mathrm{d}(\theta_2-\theta_1)}{\mathrm{d}t} + K(\theta_2-\theta_1) = T_1(t) \tag{3.2}$$

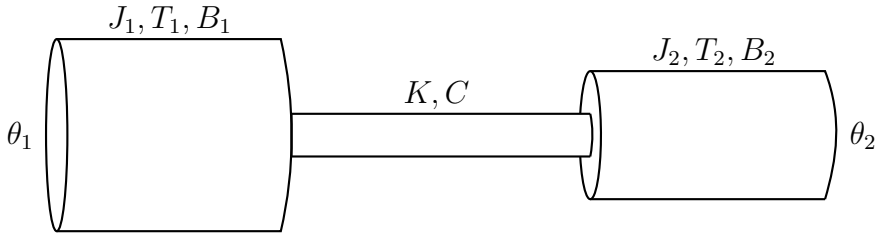

Figure 3.2: Lumped model for two mass system

where the detailed explanation of the terms are

$J_1\frac{\mathrm{d}^2\theta_1}{\mathrm{d}t^2}, J_2\frac{\mathrm{d}^2\theta_2}{\mathrm{d}t^2}$	:Torque for accelerating the masses
$B_1\frac{\mathrm{d}\theta_1}{\mathrm{d}t}, B_2\frac{\mathrm{d}\theta_2}{\mathrm{d}t}$	:Friction torque
$C\frac{\mathrm{d}(\theta_2-\theta_1)}{\mathrm{d}t}, C\frac{\mathrm{d}(\theta_2-\theta_1)}{\mathrm{d}t}$	:Viscous damping torque
$K(\theta_1-\theta_2), K(\theta_2-\theta_1)$	:Spring constant
$T_1(t), T_2(t)$	:External torques acting on the masses

Eq. (3.1)–(3.2) are coupled with the presence of derivatives of two unknown variables. Therefore, to uncouple them both Eq. (3.1) and Eq. (3.2) are added, and secondly Eq. (3.1) is multiplied by J_2 and Eq. (3.2) by J_1, then finally subtracted. Usually, the friction is neglected ($B_1 = B_2 = 0$). These simplification results into

$$J_1\frac{\mathrm{d}^2\theta_1}{\mathrm{d}t^2} + J_2\frac{\mathrm{d}^2\theta_2}{\mathrm{d}t^2} = T_1(t) + T_2(t) \tag{3.3}$$

$$J_1J_2\frac{\mathrm{d}^2(\theta_2-\theta_1)}{\mathrm{d}t^2} + (J_1+J_2)C\frac{\mathrm{d}(\theta_1-\theta_2)}{\mathrm{d}t} + (J_1+J_2)K(\theta_1-\theta_2) = J_2T_1(t) - J_1T_2(t) \tag{3.4}$$

Now, with the introduction of new variables leads to two uncoupled equations

$$(J_1+J_2)\frac{\mathrm{d}^2\Theta}{\mathrm{d}t^2} = T_1(t) + T_2(t) \tag{3.5}$$

$$\frac{J_1J_2}{J_1+J_2}\frac{\mathrm{d}^2\delta}{\mathrm{d}t^2} + C\frac{\mathrm{d}\delta}{\mathrm{d}t} + K\delta = \frac{J_2T_1(t) - J_1T_2(t)}{J_1+J_2} \tag{3.6}$$

where,

$$\begin{cases} \theta_1 - \theta_2 = \delta \\ J_1\theta_1 + J_2\theta_2 = (J_1+J_2)\Theta \end{cases} \quad \text{and} \quad \begin{cases} \theta_1 = \Theta + \dfrac{J_2}{J_1+J_2}\delta \\ \theta_2 = \Theta - \dfrac{J_1}{J_1+J_2}\delta \end{cases}$$

Eq. (3.5) describes the motion of the center of the masses of inertia, and Eq. (3.6) describes the relative motion between the two masses of inertia. Eq. (3.6)

represents the dynamics of torsion vibration, and here onward we call δ the torsion angle. Further simplification of Eq. (3.6) result in

$$J_\mu \frac{\mathrm{d}^2\delta}{\mathrm{d}t^2} + C\frac{\mathrm{d}\delta}{\mathrm{d}t} + K\delta = T_\mu \tag{3.7}$$

where, $J_\mu = \dfrac{J_1 J_2}{J_1 + J_2}$ and $T_\mu = \dfrac{J_2 T_1(t) - J_1 T_2(t)}{J_1 + J_2}$

Eq. (3.5) and Eq. (3.6) can be transformed into system of first-order differential equation and finally to the state-space format as

$$\begin{cases} \dfrac{\mathrm{d}\Omega_\Theta}{\mathrm{d}t} = \dfrac{T_1(t) + T_2(t)}{J_1 + J_2} \\ \dfrac{\mathrm{d}\Theta}{\mathrm{d}t} = \Omega_\Theta \\ \dfrac{\mathrm{d}\omega_\delta}{\mathrm{d}t} = -\dfrac{C}{J_\mu}\omega_\delta - \dfrac{K}{J_\mu}\delta + \dfrac{J_2 T_1(t) - J_1 T_2(t)}{J_1 J_2} \\ \dfrac{\mathrm{d}\delta}{\mathrm{d}t} = \omega_\delta \end{cases} \tag{3.8}$$

where, Ω_Θ is the combined angular speed, Θ is the combined rotation angle, and ω_δ is the torsional velocity [13].

3.3 Natural Frequencies and Modes

The foremost interest in analyzing any torsional system is to calculate natural frequencies and associated mode shapes. There are various techniques which could be used in determining the torsional natural frequencies; e.g. Matrix eigenvalue method, Transfer matrix method, Jacobi method, Holzer method, Finite element method (FEM) etc. Among the previously mentioned methods FEM would be the most accurate but computationally expensive method. However, a compromise is made for accuracy, and for quick determination of natural frequencies using lumped inertia model, matrix eigenvalue method have been preferred in this analysis.

The natural frequencies of the system with single shaft and two inertia can be calculated assuming no air friction ($B_1 = B_2 = 0$) and zero damping ($C = 0$). Generally, the damping provided by the steel shaft is small and could be neglected in calculation of torsional natural frequencies and mode shapes [2]. Eq. (3.1) and Eq. (3.2) then reduces to the form

$$J_1 \frac{\mathrm{d}^2\theta_1}{\mathrm{d}t^2} + K(\theta_1 - \theta_2) = 0 \tag{3.9}$$

$$J_2 \frac{\mathrm{d}^2\theta_2}{\mathrm{d}t^2} + K(\theta_2 - \theta_1) = 0 \tag{3.10}$$

In matrix form

$$\begin{bmatrix} J_1 & 0 \\ 0 & J_2 \end{bmatrix} \begin{bmatrix} \ddot{\theta}_1 \\ \ddot{\theta}_2 \end{bmatrix} + \begin{bmatrix} K & -K \\ -K & K \end{bmatrix} \begin{bmatrix} \theta_1 \\ \theta_2 \end{bmatrix} = 0 \tag{3.11}$$

Using the so called mathematical trick of solving differential equations, let the trial harmonic solution of Eq. (3.9) and Eq. (3.10) be $\theta_1 = \mathrm{Re}\{\underline{\theta}_a e^{\mathrm{j}\omega t}\}$ and $\theta_2 = \mathrm{Re}\{\underline{\theta}_b e^{\mathrm{j}\omega t}\}$. Also, assuming that the oscillation frequency remains the same for all angles. Substituting trial solution in Eq. (3.11) will result in

$$\left\{-\omega^2 \begin{bmatrix} J_1 & 0 \\ 0 & J_2 \end{bmatrix} + \begin{bmatrix} K & -K \\ -K & K \end{bmatrix}\right\} \begin{bmatrix} \underline{\theta}_{\mathrm{a}} \\ \underline{\theta}_{\mathrm{b}} \end{bmatrix} e^{\mathrm{j}\omega t} = 0 \tag{3.12}$$

Since, $e^{\mathrm{j}\omega t}$ cannot be zero, the non-zero solution exists if the determinant of the co-efficient matrix is zero. This is actually referred to eigenvalue problem in mathematics. Let $\lambda = \omega^2$, $[\mathbf{M}]$ be the mass matrix, $[\mathbf{K}]$ the stiffness matrix, and $[\theta]$ the column vector of angles. Eq. (3.12) then reduces to form

$$\{[\mathbf{K}] - \lambda\,[\mathbf{M}]\}\,[\theta] = 0 \tag{3.13}$$

Further, multiplying both sides of Eq. (3.13) by $[\mathbf{M}]^{-\mathbf{1}}$ we get

$$\{[\mathbf{A}] - \lambda\,[\mathbf{I}]\}\,[\theta] = 0 \tag{3.14}$$

Where, matrix $[\mathbf{A}] = [\mathbf{M}]^{-\mathbf{1}}[\mathbf{K}]$ is the system matrix, and $[\mathbf{I}]$ represent the identity matrix. The non-zero solution can be obtained only if $det\,([\mathbf{A}] - \lambda\,[\mathbf{I}]) = 0$. This gives a quadratic equation in λ written as

$$\lambda\left(\lambda - \frac{K(J_1 + J_2)}{J_1 J_2}\right) = 0 \tag{3.15}$$

The roots obtained are $\lambda_1 = 0$ and $\lambda_2 = \frac{K(J_1+J_2)}{J_1 J_2}$, this gives two natural frequencies, viz. $\omega_1 = 0$ and $\omega_2 = \pm\sqrt{\frac{K(J_1+J_2)}{J_1 J_2}} = \pm\sqrt{\frac{K}{J_\mu}}$. Now, substituting λ_1 and λ_2 consecutively in Eq. (3.13) yields two solutions,

$$\underline{\theta}_{\mathrm{a}} = \underline{\theta}_{\mathrm{b}} \tag{3.16a}$$

$$\underline{\theta}_{\mathrm{a}} = -\frac{J_2}{J_1}\underline{\theta}_{\mathrm{b}} \tag{3.16b}$$

If we denote the above solution by coefficients of their amplitude then system's natural frequencies and associated modes are

$$\omega_1 = 0; \quad \phi_1 = \begin{Bmatrix} 1 \\ 1 \end{Bmatrix} \quad \text{and} \quad \omega_2 = \pm\sqrt{\frac{K(J_1 + J_2)}{J_1 J_2}}; \quad \phi_2 = \begin{Bmatrix} 1 \\ -\frac{J_1}{J_2} \end{Bmatrix}$$

Clearly, there are two modes of vibration: mode one (ϕ_1) represents rigid body mode where the centres of masses have no relative displacements, and fair enough to mention that this is of no importance; mode two (ϕ_2) represents the case where vibration amplitude is inversely proportional to inertia but opposite in phase. Mode two here is a topic of concern and natural frequency associated with it. According to Eq. (3.16b), the small mass would vibrate with higher amplitude. Also, the point in the shaft where essentially no twisting occurs is called the node, and there is only one node associated with the fundamental mode. The graphical representation of mode shapes can be represented as shown in Fig. 3.3.

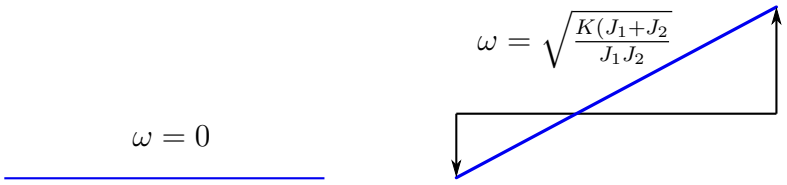

(a) Mode 1 (b) Mode 2

Figure 3.3: Mode shapes for lumped inertia model

3.4 Campbell Diagram

The most important thing in the analysis of torsional system is to identify all the potential excitation sources and their excitation frequencies; secondly, the natural frequencies of the system. Finally, this information is plotted resulting in the so-called Campbell diagram or interference diagram. The Campbell diagram gives a clear overview of the complete torsional system by aiding in identification of all potential resonant points. In Campbell diagram, frequency is plotted against the speed. In order to make a complete Campbell diagram, sources of excitations must be studied.

3.4.1 Sources of Excitation

i. Generic Sources

Generic sources arise from different mechanisms, viz. rotating unbalance, eccentricity, misalignment, and non-circular shaft cross-sections etc. These give rise to excitations at 1X[2] and 2X. Also, it is a common practice to include these excitations in almost all torsional systems [5].

ii. Induction Machine Excitations

Induction machines are essentially non-linear, as it consists of iron core. The torque produced by the machine is not smooth, as it contains harmonics, and hence this could be source of excitation. The possible excitations can be further split into two categories, viz. steady-state excitations and transient excitation. At steady-state operation fluctuations are at twice line frequency i.e. 2X. The reason behind origination of excitation at 2X is due to unsymmetrical voltage supply. The transient condition refers to starting, switch-off, and electrical faults, which result into torque excitations. Although, these transient conditions last for fraction of seconds, the magnitude of toque oscillation could be high enough to destroy the system. Start by direct supply from the grid results into high torque fluctuation. The starting torque is comprised of four components, among which two components fluctuate at line frequency while the other two are DC components [14]. The peak amplitude of the torque usually lies between 4–7 times the rated torque. The most severe type of transient excitation occur during electrical faults. An electrical fault could

[2]X is the fundamental frequency

be short circuit in the line feeding the motor, or short circuit in the machine terminal itself.

Generally, the most severe of electrical fault is considered to be two phase short circuit, and three phase short circuit. Essentially, these are the ones taken into consideration for dimensioning of the system (coupling, foundation, switchgear). The three phase short circuit essentially gives rise to torque oscillation at line frequency, whose magnitude is slightly higher than starting torque. Two phase short circuit gives rise to torque fluctuations at line frequency and twice the line frequency. And the maximum amplitude of torque lies between 5–15 times the rated air-gap torque [6].

iii. Variable Frequency Drive Excitations

Induction machines are generally used as VFD, essentially in industrial applications. However, as our torsional system consists of frequency converter, the details of this converter must be thoroughly analyzed. All VFD converters imply AC-DC-AC conversion i.e. first as rectifier and secondly as inverter. In AC-DC conversion using six-pulse diode bridge rectifier, the DC voltage comprises of six ripples per period of AC waveform. Also, if the grid supply itself is not purely balanced sinusoid then ripples at twice grid frequency are evident in addition to above ripple content. Although, there are filters included, complete elimination of these ripples is not so straight forward. Secondly, the voltage source inverter then supplies the DC voltage to the phases of induction machine. The inverter action will try to adjust the duration of the pulses fed to the machine. The variation in duration of pulses along with pulse height variation influences the air-gap flux in the machine, and essentially this leads to torque ripple. Hence, the rectifier-inverter operation is the main cause of torque ripple in the frequency converter fed machine. The same applies for PWM method and CSI fed machines [6]. However, as compared to PWM inverter and VSI, the amplitude of torque pulsation is much larger in case of CSI fed drives [15].

The excitation originating from VFD can be further sub-divided into two categories: Harmonic excitation and Inter-harmonic excitation. The excitations at the integer multiple of the supply frequency are called harmonic excitation. These excitations are at 6X, 12X, 18X, 24X etc. of the supply frequency, which are essentially present in all kind of frequency converter fed drive i.e. CSI and VSI. Inter-harmonic excitations are present in VSI drive due to non-ideal behaviour in the PWM modulation and DC voltage ripple. Inter-harmonic excitation at 2X and its multiple are also present, which is mainly due to supply asymmetry. The general formula for integer and inter-harmonic frequencies can be expressed as [6]

$$f = |kf_1 + mf_{line}| \tag{3.17}$$

where, f_1 is the inverter's output frequency, f_{line} is the grid supply frequency, k is a positive integer, and m is a positive and negative integer. The most

important of the inter-harmonic excitation are obtained when $k = 0, 6$ or 12, and $m = -2$ or -6.

The power associated with higher-order excitation is very small, hence they can be neglected. Also, the filter circuit in converters attenuates the higher frequency components. Now a complete interference diagram for a 50 Hz supply system can be formulated as shown in Fig. 3.4.

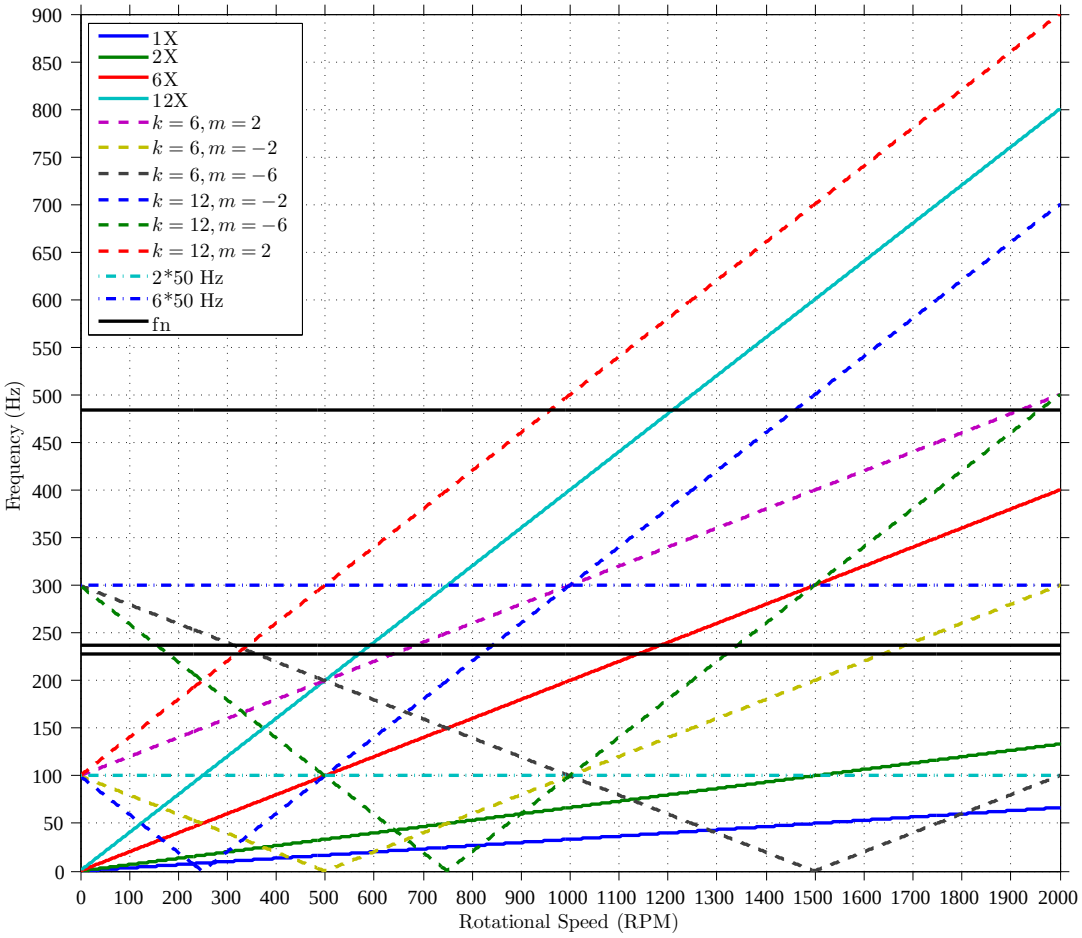

Figure 3.4: Campbell diagram for the complete system

The rotational speed in Fig. 3.4 corresponds to a four pole machine. It can be noticed that, to evade the coincidence with any excitation line shown in Campbell diagram is not so straight forward. The natural frequency below the supply frequency seems highly prone to interfere with excitation lines. Usually, the machine is accelerated quickly through these regions.

3.5 Torsional Stiffness and Damping

3.5.1 Torsional Stiffness

The torsional stiffness of the cylindrical shaft can be calculated using the following expression

$$K = \frac{\pi G D^4}{32L} \tag{3.18}$$

where, G is the shear modulus, D is the diameter of the shaft, and L is the axial length. As the stiffness is proportional to the fourth power of diameter, the shaft section close to the coupling and the drive-end journal are most flexible, and dominate the motor contribution to the coupling mode. Also, if K_1, K_2, and K_{C} be the torsional stiffness of rotor shaft of machine 1, machine 2, and coupling as shown in Fig. 2.1, then the total equivalent stiffness of the system can be calculated as

$$\frac{1}{K} = \frac{1}{K_1} + \frac{1}{K_2} + \frac{1}{K_C}$$

$$K = \frac{K_1 K_2 K_C}{K_1 K_2 + K_2 K_C + K_C K_1} \approx K_C$$

For analysis purposes coupling would be most flexible where most of the twisting would occur. In torsional analysis of two rotor inertia coupled via a flexible coupling, the stiffness related to rotor shafts can be neglected, and hence the equivalent stiffness of the system could be taken to be that of the coupling [5].

Electromagnetic Stiffness

Referring to Fig. 1.1, the electromagnetic system contributes to the stiffness of the system. The real part of the result represents the electromagnetic stiffness at particular frequency of oscillation [17]. Any disturbance in the rotor position angle will be countered by the electromagnetic system i.e it tries to bring the rotor in its actual position as it was before the disturbance. This behaviour may ultimately result in change of natural frequency. In addition, the electromagnetic stiffness could increase the natural frequency of the coupling mode to some extent [6].

3.5.2 Damping

Damping is essentially present in all torsional systems. Damping refers to dissipation of energy from the vibration mode. The effect of damping is immediate at resonance, resulting in both limited oscillation and amplification. However, determining the accurate damping value and correct measurement is not so straight forward. This leads to somehow inaccuracy in analysis. Most of the system damping is provided by the coupling, and the effect changes on each mode [15]. This might be slightly optimistic to present coupling's domination in damping, because system involving electrical machines have inherently electromagnetic damping playing a vital role [6]. Generally, component damping is expressed by a dimensionless number (usually in

percent), ζ, which is the ratio of actual damping coefficient, C, and critical damping coefficient, C_c. The critical damping, C_c, is related to the modal stiffness and modal inertia expressed as

$$C = \zeta C_c$$
$$C_c = 2\sqrt{K_0 I_0}$$

where, K_0 is the stiffness, and I_0 is the inertia of the associated mode. Hence, the damping of each component differs with changing natural frequency.

Internal Damping
Internal damping present in an un-geared VSD system is quite small. There are many authors providing empirical values of damping ratio ranging from 0.4 percent to 6 percent for un-geared systems. However, a damping ratio of one percent would be suitable for most drive train analysis [5]. This value of damping ratio will be considered throughout our study of torsional vibration.

External Damping
Since, the system under study represented by Fig. 3.1 does not include any active external dampers, further analysis and study will be limited to internal damping only. However, we take into consideration the electromagnetic damping. In studies related to torsional analysis contribution of electromagnetic system to the total stiffness and damping is left out [6]. The reason could probably be due to the complexity involved in analysing coupled electromagnetic-mechanical system.

Electromagnetic Damping
Referring to the simulation result of 37 kW cage-induction machine shown in Fig. 1.1, the electromagnetic system essentially contributes to both stiffness and damping. Except for the operation region near synchronous speed, the damping provided by the system is positive. Hence, on those regions system tries to restrict the oscillation. Nevertheless, the result shows typical behaviour in the frequency range of 40 Hz – 50 Hz where the damping essentially is negative. The simulation result shows that the value of electromagnetic damping is dependent on the frequency of oscillation, which is the frequency of forcing function.

3.6 Harmonic Excitation

In a torsion vibration analysis including VFD it may not be possible to get rid of all the interference points, as can be seen from Fig. 3.4. So, in-order to see the effect of any exciting source, a forced vibration analysis is usually done [5]. Eq. (3.7) gives the dynamics of torsion vibration. The forcing function represented as $T_\mu = \hat{T}_{\mu 0}\cos(\omega t + \gamma) = \mathrm{Re}(\underline{T}_\mu e^{\mathrm{j}\omega t})$ is applied to the system, and hence the resulting steady-state trial solution can be written as $\delta = \mathrm{Re}(\underline{\delta} e^{\mathrm{j}\omega t})$.

Substituting these trail functions in Eq. (3.7) we get,

$$\begin{aligned} -\omega^2 J_\mu \underline{\delta} e^{\mathrm{j}\omega t} + \mathrm{j}\omega C \underline{\delta} e^{\mathrm{j}\omega t} + K \underline{\delta} e^{\mathrm{j}\omega t} &= \underline{T}_\mu e^{\mathrm{j}\omega t} \\ \left(-\omega^2 J_\mu + \mathrm{j}\omega C + K\right) \underline{\delta} e^{\mathrm{j}\omega t} &= \underline{T}_\mu e^{\mathrm{j}\omega t} \\ \underline{\delta} &= \frac{\underline{T}_\mu}{(K - \omega^2 J_\mu) + \mathrm{j}\omega C} \end{aligned} \tag{3.19}$$

Often damping is expresses in terms of damping ratio, (ζ), equivalent mass moment of inertia, (J_μ), and natural frequency (ω_n) as $C = \zeta C_\mathrm{c} = 2\zeta J_\mu \omega_\mathrm{n}$. The natural frequency can be written as $\omega_\mathrm{n}^2 = K/J_\mu$. Substituting these changes in Eq. (3.19), the frequency response between torsion angle and excitation torque can be written as

$$\frac{\underline{\delta}}{\underline{T}_\mu} = \frac{\dfrac{1}{K}}{1 - \left(\dfrac{\omega}{\omega_\mathrm{n}}\right)^2 + \mathrm{j}2\zeta\dfrac{\omega}{\omega_\mathrm{n}}} \tag{3.20}$$

3.6.1 Shaft-end Torque

The harmonic torque acting on the masses are not exactly replicated at the shaft-end connecting the masses. Using Eq. (3.20) the shaft-end torque can be expressed as

$$\begin{aligned} T_\mathrm{shaft} &= K\delta \\ &= \hat{T}_{\mu 0} \frac{1}{\sqrt{\left(1 - \dfrac{\omega^2}{\omega_\mathrm{n}^2}\right)^2 + \left(2\zeta\dfrac{\omega}{\omega_\mathrm{n}}\right)^2}} \cos(\omega t + \gamma) \end{aligned} \tag{3.21}$$

where,

$$\gamma = \arctan \frac{2\zeta\omega_\mathrm{n}\omega}{\omega_\mathrm{n}^2 - \omega^2}$$

Eq. (3.21) is the torque transmitted in the shaft of the drive system [16]. Usually, the peak amplitude of this torque determines the foundation and coupling requirements. The importance of the damping can be studied from Eq. (3.21), where, the amplification factor is essentially dependent on the damping ratio when $\omega = \omega_\mathrm{n}$. Hence, damping is highly beneficial near resonance.

3.7 Exciter Selection

The following step by step procedure was followed in order to dimension the exciter machine

i. Moment of inertia (J_1) of 37 kW cage induction machine (test machine) is known

ii. Torsional stiffness (K) is known from the coupling, the type of coupling to be used is essentially fixed

iii. Campbell diagram for the proposed torsional system is formulated

iv. The region of very low interference possibility and the natural frequency above 100 Hz is checked from the Campbell diagram

v. Natural frequency of some value above 100 Hz can be assumed

vi. Expression for natural frequency is used to determine the mass moment of inertia (J_2) of exciter machine

vii. The newly obtained value of moment of inertia for exciter machine (J_2) is compared with the available machine specifications provided by the manufacturer

Also, from the Campbell diagram shown in Fig. 3.4, the region between 100 Hz to 300 Hz has very low possibility of getting interference between the natural frequency and the excitation line, except at 100 Hz, 200 Hz and 300 Hz itself. The study region lies between 0 Hz – 100 Hz, hence choosing natural frequency above 100 Hz could be one possibility to find the mass moment of inertia of the exciter machine. Essentially, the mass moment of inertia of the test machine under study is fixed. Using the expression for natural frequency of the two mass system we get

$$J_2 = \frac{K}{\omega_{\mathrm{n}}^2 - \dfrac{K}{J_1}} \tag{3.22}$$

Induction machine corresponding to value of rotor inertia obtained from Eq. (3.22) will be sorted out from the available ratings. If the machine corresponding to above obtained value of rotor inertia is not available then higher rating will be preferred, and hence the natural frequency will be re-calculated using this inertia. The possible layout of the exciter is shown in Fig. 3.5.

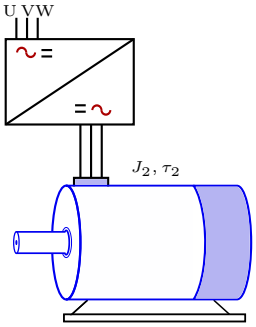

Figure 3.5: Exciter set-up

The second part involves choosing appropriate frequency converter having proper control algorithm for the production of sinusoidal air-gap torque. The algorithm must allow tuning both peak amplitude and frequency of the air-gap torque. Also, a condition where the harmonic excitation is superimposed on a DC value of torque will also be considered.

4 Small-signal Model

The main aim is to study the stability of the proposed torsional system, and therefore, it is essential to linearize the coupled electromagnetic-mechanical system, and use the eigenvalue method to study the system behaviour. Secondly, we need to formulate an analytical model for verifying simulation result of Fig. 1.1. So, small-signal model would be the straight forward procedure to achieve our aim. Small-signal model is formulated within space vector model of cage-induction machine.

4.1 Space Vector Model of Cage-induction Machine

Transient analysis is often regarded as difficult, as it deals with non-linear equations, and formulation of analytical models is somehow a cumbersome task. To perform the dynamic analysis of AC machines, space vector model is usually used due to its fast result. Pal K. Kovacs [14] has provided with the space vector formulation for analysing transients in induction machine. Unlike finite element analysis, space vector model does not include effect of saturation. The four basic assumptions of space vector theory are

i. Sinusoidal distribution of air-gap flux density along the air-gap of machine

ii. Linear magnetization curve

iii. Iron losses are neglected

iv. Temperature and frequency dependency of resistances and inductances are not taken into account

The stator and rotor voltage equations in a reference frame rotating at speed ω_k can be written as

$$\underline{u}_\mathrm{s}^\mathrm{k} = \underline{i}_\mathrm{s}^\mathrm{k} R_\mathrm{s} + \frac{\mathrm{d}\underline{\psi}_\mathrm{s}^\mathrm{k}}{\mathrm{d}t} + \mathrm{j}\omega_\mathrm{k}\underline{\psi}_\mathrm{s}^\mathrm{k} \tag{4.1}$$

$$\underline{u}_\mathrm{r}^\mathrm{k} = \underline{i}_\mathrm{r}^\mathrm{k} R_\mathrm{r} + \frac{\mathrm{d}\underline{\psi}_\mathrm{r}^\mathrm{k}}{\mathrm{d}t} + \mathrm{j}(\omega_\mathrm{k} - \omega)\underline{\psi}_\mathrm{r}^\mathrm{k} \tag{4.2}$$

where,

$\underline{i}_\mathrm{s}^\mathrm{k} R_\mathrm{s}$, $\underline{i}_\mathrm{r}^\mathrm{k} R_\mathrm{r}$	:Resistive drop in stator and rotor coils
$\frac{\mathrm{d}\underline{\psi}_\mathrm{s}^\mathrm{k}}{\mathrm{d}t}$, $\frac{\mathrm{d}\underline{\psi}_\mathrm{r}^\mathrm{k}}{\mathrm{d}t}$	:Induced emf due to changing flux-linkage
$\mathrm{j}\omega_\mathrm{k}\underline{\psi}_\mathrm{s}^\mathrm{k}$, $\mathrm{j}(\omega_\mathrm{k} - \omega)\underline{\psi}_\mathrm{s}^\mathrm{k}$	:Motional emf

Also, to be mentioned both ω_k and ω are expressed in electrical degrees. The flux-linkage can be expressed in terms of currents as,

$$\underline{\psi}_\mathrm{s}^\mathrm{k} = L_\mathrm{s}\underline{i}_\mathrm{s}^\mathrm{k} + L_\mathrm{m}\underline{i}_\mathrm{s}^\mathrm{k} \tag{4.3}$$

$$\underline{\psi}_\mathrm{r}^\mathrm{k} = L_\mathrm{m}\underline{i}_\mathrm{s}^\mathrm{k} + L_\mathrm{r}\underline{i}_\mathrm{r}^\mathrm{k} \tag{4.4}$$

where, L_s and L_r are the total inductance of the stator and rotor windings. Also, L_m represents the magnetizing inductance. The total inductances can be represented as a sum of magnetizing inductance and leakage inductance as follows

$$\begin{cases} L_\mathrm{s} = L_{\mathrm{s}\sigma} + L_\mathrm{m} \\ L_\mathrm{r} = L_{\mathrm{r}\sigma} + L_\mathrm{m} \end{cases} \tag{4.5}$$

Since, the dynamic equation consists of four variables: two flux-linkages and two currents; it would be wise to put them in any of two variables. And this can be done by using Eq. (4.3) and Eq. (4.4) respectively. The stator and rotor currents in terms of stator and rotor flux-linkages can be expressed as

$$\underline{i}_\mathrm{s}^\mathrm{k} = \frac{\underline{\psi}_\mathrm{s}^\mathrm{k} - \dfrac{L_\mathrm{m}}{L_\mathrm{r}}\underline{\psi}_\mathrm{r}^\mathrm{k}}{L_\mathrm{s} - \dfrac{L_\mathrm{m}^2}{L_\mathrm{r}}} = \frac{\underline{\psi}_\mathrm{s}^\mathrm{k} - K_\mathrm{r}\underline{\psi}_\mathrm{r}^\mathrm{k}}{L'_\mathrm{s}} \tag{4.6}$$

$$\underline{i}_\mathrm{r}^\mathrm{k} = \frac{\underline{\psi}_\mathrm{r}^\mathrm{k} - \dfrac{L_\mathrm{m}}{L_\mathrm{s}}\underline{\psi}_\mathrm{s}^\mathrm{k}}{L_\mathrm{r} - \dfrac{L_\mathrm{m}^2}{L_\mathrm{s}}} = \frac{\underline{\psi}_\mathrm{r}^\mathrm{k} - K_\mathrm{s}\underline{\psi}_\mathrm{s}^\mathrm{k}}{L'_\mathrm{r}} \tag{4.7}$$

where, K_s and K_r are the stator and rotor coupling factors, while L'_s and L'_r are the transient inductances of stator and rotor respectively.

Substituting Eq. (4.6) and Eq. (4.7) in voltage Eq. (4.1) and Eq. (4.2) will result in equations with only flux-linkages as free variables, also included is angular speed. The resulting equations are

$$\underline{u}_\mathrm{s}^\mathrm{k} = \left(\frac{R_\mathrm{s}}{L'_\mathrm{s}} + \mathrm{j}\omega_\mathrm{k}\right)\underline{\psi}_\mathrm{s}^\mathrm{k} - K_\mathrm{r}\frac{R_\mathrm{s}}{L'_\mathrm{s}}\underline{\psi}_\mathrm{r}^\mathrm{k} + \frac{\mathrm{d}\underline{\psi}_\mathrm{s}^\mathrm{k}}{\mathrm{d}t} \tag{4.8}$$

$$\underline{u}_\mathrm{r}^\mathrm{k} = -K_\mathrm{r}\frac{R_\mathrm{r}}{L'_\mathrm{r}}\underline{\psi}_\mathrm{s}^\mathrm{k} + \left[\frac{R_\mathrm{r}}{L'_\mathrm{r}} + \mathrm{j}(\omega_\mathrm{k} - \omega)\right]\underline{\psi}_\mathrm{r}^\mathrm{k} + \frac{\mathrm{d}\underline{\psi}_\mathrm{r}^\mathrm{k}}{\mathrm{d}t} \tag{4.9}$$

The electromagnetic torque can also be expressed as

$$\tau_\mathrm{e} = \frac{3}{2}p\frac{K_\mathrm{r}}{L'_\mathrm{s}}\mathrm{Im}\{\underline{\psi}_\mathrm{r}^{\mathrm{k}*}\underline{\psi}_\mathrm{s}\} \tag{4.10}$$

4.2 Steady-state Operation

The steady-state voltage equations of cage-induction machine can be obtained by substituting the steady state quantities in the dynamic equation. Also, if the reference frame taken is rotating at synchronous speed then $\omega_\mathrm{k} = \omega_\mathrm{s}$. The steady state voltage equations can be expressed as

$$\underline{u}_{\mathrm{s}0}^\mathrm{k} = \underline{i}_{\mathrm{s}0}^\mathrm{k} R_\mathrm{s} + \mathrm{j}\omega_\mathrm{s}\underline{\psi}_{\mathrm{s}0}^\mathrm{k} \tag{4.11}$$

$$\underline{u}_{\mathrm{r}0}^\mathrm{k} = \underline{i}_{\mathrm{r}0}^\mathrm{k} R_\mathrm{r} + \mathrm{j}(\omega_\mathrm{s} - \omega_0)\underline{\psi}_{\mathrm{r}0}^\mathrm{k} \tag{4.12}$$

In steady state condition, the derivative term vanishes and rotor rotates at constant speed. Now, the slip of the machine can be defined as the difference between the speed of reference frame and rotor speed as

$$S = \frac{\omega_\mathrm{s} - \omega}{\omega_\mathrm{s}}$$

Using Eq. (4.3)–(4.5) the steady state flux equations becomes

$$\begin{cases} \underline{\psi}^\mathrm{k}_\mathrm{s0} = L_{\mathrm{s}\sigma}\underline{i}^\mathrm{k}_\mathrm{s0} + L_\mathrm{m}(\underline{i}^\mathrm{k}_\mathrm{s0} + \underline{i}^\mathrm{k}_\mathrm{r0}) \\ \underline{\psi}^\mathrm{k}_\mathrm{r0} = L_{\mathrm{r}\sigma}\underline{i}^\mathrm{k}_\mathrm{r0} + L_\mathrm{m}(\underline{i}^\mathrm{k}_\mathrm{s0} + \underline{i}^\mathrm{k}_\mathrm{r0}) \end{cases} \tag{4.13}$$

Substituting the steady state flux-linkages from Eq. (4.13) into steady state voltage Eq. (4.11) and Eq. (4.12) will result into

$$\underline{u}^\mathrm{k}_\mathrm{s0} = \underline{i}^\mathrm{k}_\mathrm{s0}R_\mathrm{s} + \mathrm{j}X_{\mathrm{s}\sigma}\underline{i}^\mathrm{k}_\mathrm{s0} + \mathrm{j}X_\mathrm{m}(\underline{i}^\mathrm{k}_\mathrm{s0} + \underline{i}^\mathrm{k}_\mathrm{r0}) \tag{4.14}$$

$$0 = \underline{i}^\mathrm{k}_\mathrm{r0}\frac{R_\mathrm{r}}{S} + \mathrm{j}X_{\mathrm{r}\sigma}\underline{i}^\mathrm{k}_\mathrm{r0} + \mathrm{j}X_\mathrm{m}(\underline{i}^\mathrm{k}_\mathrm{s0} + \underline{i}^\mathrm{k}_\mathrm{r0}) \tag{4.15}$$

Two unknowns provided with two equations can be solved with ease. Therefore, the steady state currents obtained are

$$\underline{i}^\mathrm{k}_\mathrm{s0} = \frac{R_\mathrm{r} + \mathrm{j}X_\mathrm{r}}{R_\mathrm{s}R_\mathrm{r} - S\sigma X_\mathrm{s}X_\mathrm{r} + \mathrm{j}(R_\mathrm{r}X_\mathrm{s} + SR_\mathrm{s}X_\mathrm{r})}\underline{u}^\mathrm{k}_\mathrm{s0} \tag{4.16}$$

$$\underline{i}^\mathrm{k}_\mathrm{r0} = \frac{-\mathrm{j}SX_\mathrm{m}}{R_\mathrm{s}R_\mathrm{r} - S\sigma X_\mathrm{s}X_\mathrm{r} + \mathrm{j}(R_\mathrm{r}X_\mathrm{s} + SR_\mathrm{s}X_\mathrm{r})}\underline{u}^\mathrm{k}_\mathrm{s0} \tag{4.17}$$

where, $\begin{cases} X_{\mathrm{s}\sigma} = \omega_\mathrm{s}L_{\mathrm{s}\sigma} \\ X_{\mathrm{r}\sigma} = \omega_\mathrm{s}L_{\mathrm{r}\sigma} \\ X_\mathrm{s} = \omega_\mathrm{s}L_\mathrm{s} \\ X_\mathrm{r} = \omega_\mathrm{s}L_\mathrm{r} \end{cases}$ and $\begin{cases} X_\mathrm{m} = \omega_\mathrm{s}L_\mathrm{m} \\ \sigma = \dfrac{X_\mathrm{s}X_\mathrm{r} - {X_\mathrm{m}}^2}{X_\mathrm{s}X_\mathrm{r}} \end{cases}$

The stator supply voltage in stator frame of reference can be expressed as

$$\underline{u}^s_\mathrm{s0} = \hat{u}_s e^{\mathrm{j}(\omega_\mathrm{s}t + \varphi_u)}$$

Let, the speed of the arbitrarily chosen reference frame be equal to the synchronous speed i.e. $\omega_\mathrm{k} = \omega_\mathrm{s}$, then the position angle of the chosen reference frame can be expressed as

$$\vartheta_k = \vartheta_{k0} + \int_0^t \omega_\mathrm{s}dt = \omega_\mathrm{s}t$$

Eventually, the transformation of stator voltage from stator reference frame into chosen reference frame can be expressed as

$$\underline{u}^\mathrm{k}_\mathrm{s0} = \underline{u}^s_\mathrm{s0}e^{-\mathrm{j}\vartheta} = \hat{u}_s e^{\mathrm{j}(\omega_\mathrm{s}t + \varphi_u)}e^{-\mathrm{j}\omega_\mathrm{s}t} = \hat{u}_s e^{\mathrm{j}\varphi_u} \tag{4.18}$$

Hence, the steady-state stator voltage is simply a constant vector in the chosen reference frame.

Also, the steady state electromagnetic torque can be expressed as

$$\tau_{e0} = \frac{3}{2} p \frac{K_r}{L_s'} \mathrm{Im}\{\underline{\psi}_{r0}^{k\,*} \underline{\psi}_{s0}\} \tag{4.19}$$

The steady-state flux-linkage can be resolved into its real and imaginary component and hence the steady-state torque equation can be re-written as

$$\tau_{e0} = \frac{3}{2} p \frac{K_r}{L_s'} (\psi_{rx0}\psi_{sy0} - \psi_{ry0}\psi_{sx0}) \tag{4.20}$$

The steady-state values will be needed later while performing small-signal analysis.

4.3 Small-signal Analysis

The dynamic equation of induction machine is non-linear as it inherently consists of product of two variables i.e. speed and flux-linkage, also the torque equation is non-linear in the same respect. One of the possibilities is to linearise the system by adding small perturbation to the steady state variables near the steady-state point. The other possibility is to directly solve the system using some numerical method like Trapezoidal, Runge–Kutta, etc.

A small perturbation added to the steady-state variables can be represented as

$$\begin{aligned} \underline{\psi}_s &= \underline{\psi}_{s0} + \Delta\underline{\psi}_s \quad ; \quad \underline{u}_s = \underline{u}_{s0} + \Delta\underline{u}_s \quad ; \quad \tau_e = \tau_{e0} + \Delta\tau_e \\ \underline{\psi}_r &= \underline{\psi}_{r0} + \Delta\underline{\psi}_r \quad ; \quad \underline{u}_r = \underline{u}_{r0} + \Delta\underline{u}_r \quad ; \quad \omega = \omega_0 + \Delta\omega \end{aligned}$$

Substituting these perturbation in Eq. (4.8), Eq. (4.9), and Eq. (4.10) result into

$$\underline{u}_{s0} + \Delta\underline{u}_s = \left(\frac{R_s}{L_s'} + \mathrm{j}\omega_k\right)(\underline{\psi}_{s0} + \Delta\underline{\psi}_s) - K_r \frac{R_s}{L_s'}(\underline{\psi}_{r0} + \Delta\underline{\psi}_r) + \frac{\mathrm{d}(\underline{\psi}_{s0} + \Delta\underline{\psi}_s)}{\mathrm{d}t} \tag{4.21}$$

$$\begin{aligned} \underline{u}_{r0} + \Delta\underline{u}_r = -K_r \frac{R_r}{L_r'}(\underline{\psi}_{s0} + \Delta\underline{\psi}_s) + \left[\frac{R_r}{L_r'} + \mathrm{j}(\omega_k - (\omega_0 + \Delta\omega))\right](\underline{\psi}_{r0} + \Delta\underline{\psi}_r) \\ + \frac{\mathrm{d}(\underline{\psi}_{r0} + \Delta\underline{\psi}_r)}{\mathrm{d}t} \end{aligned} \tag{4.22}$$

$$\tau_{e0} + \Delta\tau_e = \frac{3}{2} p \frac{K_r}{L_s'} \mathrm{Im}\{(\underline{\psi}_{r0} + \Delta\underline{\psi}_r)^*(\underline{\psi}_{s0} + \Delta\underline{\psi}_s)\} \tag{4.23}$$

The steady-state voltage and torque equations can be expressed as

$$\begin{cases} \underline{u}_{s0} = \left(\dfrac{R_s}{L_s'} + \mathrm{j}\omega_k\right)\underline{\psi}_{s0} - K_r \dfrac{R_s}{L_s'}\underline{\psi}_{r0} \\ \underline{u}_{r0} = -K_r \dfrac{R_r}{L_r'}\underline{\psi}_{s0} + \left[\dfrac{R_r}{L_r'} + \mathrm{j}(\omega_k - \omega_0)\right]\underline{\psi}_{r0} \end{cases} \tag{4.24}$$

Now, subtracting the steady state Eq. (4.20), Eq. (4.24) from Eq. (4.21)–Eq. (4.23) consisting of small perturbation result into

$$\Delta\underline{u}_s = \left(\frac{R_s}{L_s'} + \mathrm{j}\omega_k\right)\Delta\underline{\psi}_s - K_r \frac{R_s}{L_s'}\Delta\underline{\psi}_r + \frac{\mathrm{d}\Delta\underline{\psi}_s}{\mathrm{d}t} \tag{4.25}$$

$$0 = -K_{\mathrm{r}}\frac{R_{\mathrm{r}}}{L_{\mathrm{r}}'}\Delta\underline{\psi}_{\mathrm{s}} + \left[\frac{R_{\mathrm{r}}}{L_{\mathrm{r}}'} + \mathrm{j}(\omega_{\mathrm{k}} - \omega_0)\right]\Delta\underline{\psi}_{\mathrm{r}} - \mathrm{j}\Delta\omega\underline{\psi}_{\mathrm{r}0} + \frac{\mathrm{d}\Delta\underline{\psi}_{\mathrm{r}}}{\mathrm{d}t} \tag{4.26}$$

$$\Delta\tau_{\mathrm{e}} = \frac{3}{2}p\frac{K_{\mathrm{r}}}{L_{\mathrm{s}}'}\mathrm{Im}\{(\underline{\psi}_{\mathrm{r}0})^*\Delta\underline{\psi}_{\mathrm{s}} + \Delta(\underline{\psi}_{\mathrm{r}})^*\underline{\psi}_{\mathrm{s}0}\} \tag{4.27}$$

Eq. (4.21)–(4.23) is now linearised. Also, while obtaining these equations the product of two small perturbations has been neglected i.e. $\Delta\omega\Delta\underline{\psi}_{\mathrm{r}} = 0$, and in case of cage-induction machine the rotor bars are short-circuited using end rings therefore, $\Delta u_{\mathrm{r}} = 0$. The voltage equations can now be written in component form and finally re-arranged into the state-space format as follows

$$\begin{cases} \dfrac{\mathrm{d}\Delta\psi_{\mathrm{sx}}}{\mathrm{d}t} = -\dfrac{R_{\mathrm{s}}}{L_{\mathrm{s}}'}\Delta\psi_{\mathrm{sx}} + \omega_{\mathrm{k}}\Delta\psi_{\mathrm{sy}} + K_{\mathrm{r}}\dfrac{R_{\mathrm{s}}}{L_{\mathrm{s}}'}\Delta\psi_{\mathrm{rx}} + \Delta u_{\mathrm{sx}} \\ \dfrac{\mathrm{d}\Delta\psi_{\mathrm{sy}}}{\mathrm{d}t} = -\omega_{\mathrm{k}}\Delta\psi_{\mathrm{sx}} - \dfrac{R_{\mathrm{s}}}{L_{\mathrm{s}}'}\Delta\psi_{\mathrm{sy}} + K_{\mathrm{r}}\dfrac{R_{\mathrm{s}}}{L_{\mathrm{s}}'}\Delta\psi_{\mathrm{ry}} + \Delta u_{\mathrm{sy}} \\ \dfrac{\mathrm{d}\Delta\psi_{\mathrm{rx}}}{\mathrm{d}t} = K_{\mathrm{s}}\dfrac{R_{\mathrm{r}}}{L_{\mathrm{r}}'}\Delta\psi_{\mathrm{sx}} - \dfrac{R_{\mathrm{r}}}{L_{\mathrm{r}}'}\Delta\psi_{\mathrm{rx}} + (\omega_{\mathrm{k}} - \omega_0)\Delta\psi_{\mathrm{ry}} - \Delta\omega\psi_{\mathrm{ry}0} \\ \dfrac{\mathrm{d}\Delta\psi_{\mathrm{ry}}}{\mathrm{d}t} = K_{\mathrm{s}}\dfrac{R_{\mathrm{r}}}{L_{\mathrm{r}}'}\Delta\psi_{\mathrm{sy}} - (\omega_{\mathrm{k}} - \omega_0)\Delta\psi_{\mathrm{rx}} - \dfrac{R_{\mathrm{r}}}{L_{\mathrm{r}}'}\Delta\psi_{\mathrm{ry}} + \Delta\omega\psi_{\mathrm{rx}0} \end{cases} \tag{4.28}$$

Also, the linearised torque Eq. (4.27) can be re-written as

$$\Delta\tau_{\mathrm{e}} = \frac{3}{2}p\frac{K_{\mathrm{r}}}{L_{\mathrm{s}}'}(-\psi_{\mathrm{ry}0}\Delta\psi_{\mathrm{sx}} + \psi_{\mathrm{rx}0}\Delta\psi_{\mathrm{sy}} + \psi_{\mathrm{sy}0}\Delta\psi_{\mathrm{rx}} - \psi_{\mathrm{sx}0}\Delta\psi_{\mathrm{ry}}) \tag{4.29}$$

The system of first-order ordinary differential Eq. (4.28) are for a single cage-induction machine. In our analysis we consider the two mass system to be two cage-induction machine as shown in Fig. 3.1. The masses represent the rotors of individual machines, whose shafts are coupled through a flexible coupling. The two coupled electrical machine is considered as single degree of freedom (SDF) torsional system. Now, the electromagnetic equations are coupled to the mechanical equations, and would require four voltage equations for each one of electrical machine, and four mechanical equations to be solved simultaneously. Hence, a total of 12 first-order ordinary differential equations represent the complete torsional system. The system of equations can finally be expressed using Eq. (3.8), Eq. (4.28), and Eq. (4.29) as follows

$$\begin{cases} \dfrac{\mathrm{d}\Delta\psi_{\mathrm{sx1}}}{\mathrm{d}t} = -\dfrac{R_{\mathrm{s1}}}{L_{\mathrm{s1}}'}\Delta\psi_{\mathrm{sx1}} + \omega_{\mathrm{k}}\Delta\psi_{\mathrm{sy1}} + K_{\mathrm{r1}}\dfrac{R_{\mathrm{s1}}}{L_{\mathrm{s1}}'}\Delta\psi_{\mathrm{rx1}} + \Delta u_{\mathrm{sx1}} \\ \dfrac{\mathrm{d}\Delta\psi_{\mathrm{sy1}}}{\mathrm{d}t} = -\omega_{\mathrm{k}}\Delta\psi_{\mathrm{sx1}} - \dfrac{R_{\mathrm{s1}}}{L_{\mathrm{s1}}'}\Delta\psi_{\mathrm{sy1}} + K_{\mathrm{r1}}\dfrac{R_{\mathrm{s1}}}{L_{\mathrm{s1}}'}\Delta\psi_{\mathrm{ry1}} + \Delta u_{\mathrm{sy1}} \\ \dfrac{\mathrm{d}\Delta\psi_{\mathrm{rx1}}}{\mathrm{d}t} = K_{\mathrm{s1}}\dfrac{R_{\mathrm{r1}}}{L_{\mathrm{r1}}'}\Delta\psi_{\mathrm{sx1}} - \dfrac{R_{\mathrm{r1}}}{L_{\mathrm{r1}}'}\Delta\psi_{\mathrm{rx1}} + (\omega_{\mathrm{k}} - \omega_{01})\Delta\psi_{\mathrm{ry1}} - (\omega_1 - \omega_{01})\psi_{\mathrm{ry0,1}} \\ \dfrac{\mathrm{d}\Delta\psi_{\mathrm{ry1}}}{\mathrm{d}t} = K_{\mathrm{s1}}\dfrac{R_{\mathrm{r1}}}{L_{\mathrm{r1}}'}\Delta\psi_{\mathrm{sy1}} - (\omega_{\mathrm{k}} - \omega_{01})\Delta\psi_{\mathrm{rx1}} - \dfrac{R_{\mathrm{r1}}}{L_{\mathrm{r1}}'}\Delta\psi_{\mathrm{ry1}} + (\omega_1 - \omega_{01})\psi_{\mathrm{rx0,1}} \end{cases} \tag{4.30}$$

$$\begin{cases} \dfrac{\mathrm{d}\Delta\psi_{\mathrm{sx2}}}{\mathrm{d}t} = -\dfrac{R_{\mathrm{s2}}}{L_{\mathrm{s2}}'}\Delta\psi_{\mathrm{sx2}} + \omega_{\mathrm{k}}\Delta\psi_{\mathrm{sy2}} + K_{\mathrm{r2}}\dfrac{R_{\mathrm{s2}}}{L_{\mathrm{s2}}'}\Delta\psi_{\mathrm{rx2}} + \Delta u_{\mathrm{sx2}} \\ \dfrac{\mathrm{d}\Delta\psi_{\mathrm{sy2}}}{\mathrm{d}t} = -\omega_{\mathrm{k}}\Delta\psi_{\mathrm{sx2}} - \dfrac{R_{\mathrm{s2}}}{L_{\mathrm{s2}}'}\Delta\psi_{\mathrm{sy2}} + K_{\mathrm{r2}}\dfrac{R_{\mathrm{s2}}}{L_{\mathrm{s2}}'}\Delta\psi_{\mathrm{ry2}} + \Delta u_{\mathrm{sy2}} \\ \dfrac{\mathrm{d}\Delta\psi_{\mathrm{rx2}}}{\mathrm{d}t} = K_{\mathrm{s2}}\dfrac{R_{\mathrm{r2}}}{L_{\mathrm{r2}}'}\Delta\psi_{\mathrm{sx2}} - \dfrac{R_{\mathrm{r2}}}{L_{\mathrm{r2}}'}\Delta\psi_{\mathrm{rx2}} + (\omega_{\mathrm{k}} - \omega_{02})\Delta\psi_{\mathrm{ry2}} - (\omega_2 - \omega_{02})\psi_{\mathrm{ry0,2}} \\ \dfrac{\mathrm{d}\Delta\psi_{\mathrm{ry2}}}{\mathrm{d}t} = K_{\mathrm{s2}}\dfrac{R_{\mathrm{r2}}}{L_{\mathrm{r2}}'}\Delta\psi_{\mathrm{sy2}} - (\omega_{\mathrm{k}} - \omega_{02})\Delta\psi_{\mathrm{rx2}} - \dfrac{R_{\mathrm{r2}}}{L_{\mathrm{r2}}'}\Delta\psi_{\mathrm{ry2}} + (\omega_2 - \omega_{02})\psi_{\mathrm{rx0,2}} \end{cases} \tag{4.31}$$

$$\begin{cases} \dfrac{\mathrm{d}\Omega_\Theta}{\mathrm{d}t} = \dfrac{\tau_{e1} + \tau_{e2}}{J_1 + J_2} \\ \dfrac{\mathrm{d}\Theta}{\mathrm{d}t} = \Omega_\Theta \\ \dfrac{\mathrm{d}\omega_\delta}{\mathrm{d}t} = -\dfrac{C}{J_\mu}\omega_\delta - \dfrac{K}{J_\mu}\delta + \dfrac{J_2\tau_{\mathrm{e1}} - J_1\tau_{\mathrm{e2}}}{J_1 J_2} \\ \dfrac{\mathrm{d}\delta}{\mathrm{d}t} = \omega_\delta \end{cases} \tag{4.32}$$

Some of the terms in Eq. (4.30)–Eq. (4.32) include electro-magnetic torque and angular speeds, which still need to be expanded in terms of the state variables.

$$\begin{cases} \omega_1 = \Omega_\Theta + \dfrac{J_2}{J_1 + J_2}\omega_\delta \\ \omega_2 = \Omega_\Theta - \dfrac{J_1}{J_1 + J_2}\omega_\delta \\ \tau_{\mathrm{e1}} = \dfrac{3}{2}p_1\dfrac{K_{r1}}{L_{s1}'}(-\psi_{\mathrm{ry0,1}}\Delta\psi_{\mathrm{sx1}} + \psi_{\mathrm{rx0,1}}\Delta\psi_{\mathrm{sy1}} + \psi_{\mathrm{sy0,1}}\Delta\psi_{\mathrm{rx1}} - \psi_{\mathrm{sx0,1}}\Delta\psi_{\mathrm{ry1}} \\ \qquad + \psi_{\mathrm{rx0,1}}\psi_{\mathrm{sy0,1}} - \psi_{\mathrm{ry0,1}}\psi_{\mathrm{sx0,1}}) \\ \tau_{\mathrm{e2}} = \dfrac{3}{2}p_2\dfrac{K_{r2}}{L_{s2}'}(-\psi_{\mathrm{ry0,2}}\Delta\psi_{\mathrm{sx2}} + \psi_{\mathrm{rx0,2}}\Delta\psi_{\mathrm{sy2}} + \psi_{\mathrm{sy0,2}}\Delta\psi_{\mathrm{rx2}} - \psi_{\mathrm{sx0,2}}\Delta\psi_{\mathrm{ry2}} \\ \qquad + \psi_{\mathrm{rx0,2}}\psi_{\mathrm{sy0,2}} - \psi_{\mathrm{ry0,2}}\psi_{\mathrm{sx0,2}}) \end{cases} \tag{4.33}$$

Subscript 1 represents 37 kW induction machine, and 2 for 4 kW induction machine, and included 0 represents steady-state parameter. Usually, the speed is given in mechanical degree which has to be converted into electrical degree. This can be done taking account of the pole-pairs of the machine. The angular speeds are then $\omega_{01} = p_1\omega_{\mathrm{m0,1}}$, and $\omega_{02} = p_2\omega_{\mathrm{m0,2}}$. Hence, all the needed parameters of the equations describing the system have more or less been described. The Eq. (4.30)–(4.32) are already in the form

$$\frac{\mathrm{d}\mathbf{x}}{\mathrm{d}t} = \mathbf{A}\mathbf{x} + \mathbf{B}\mathbf{u} \tag{4.34}$$

where, $\mathbf{A}$ and $\mathbf{B}$ are 12×12 matrix, $\mathbf{x}$ is a 12×1 column vector representing state variables. Similarly, $\mathbf{u}$ consists of the constant parameters and is also a 12×1 column

vector. Column vectors $\mathbf{x}$ and $\mathbf{u}$ are listed below, while $\mathbf{A}$ and $\mathbf{B}$ are mentioned in the Appendix A.

$$\mathbf{x} = [\Delta\psi_{\mathrm{sx1}}\ \Delta\psi_{\mathrm{sy1}}\ \Delta\psi_{\mathrm{rx1}}\ \Delta\psi_{\mathrm{ry1}}\ \Delta\psi_{\mathrm{sx2}}\ \Delta\psi_{\mathrm{sy2}}\ \Delta\psi_{\mathrm{rx2}}\ \Delta\psi_{\mathrm{ry2}}\ \Omega_\Theta\ \Theta\ \omega_\delta\ \delta]^T$$

$$\mathbf{u} = [\Delta u_{\mathrm{sx1}}\ \Delta u_{\mathrm{sy1}}\ \omega_{0,1}\psi_{\mathrm{ry0,1}}\ \ \omega_{0,1}\psi_{\mathrm{rx0,1}}\ \Delta u_{\mathrm{sx2}}\ \Delta u_{\mathrm{sy2}}\ \omega_{0,2}\psi_{\mathrm{ry0,2}}\ \ \omega_{0,2}\psi_{\mathrm{rx0,2}}\ M\ 0\ N\ 0]^T$$

where,

$$M = \frac{3p_1K_{\mathrm{r1}}}{2L_{\mathrm{s1}}'(J_1+J_2)}(\psi_{\mathrm{rx0,1}}\psi_{\mathrm{sy0,1}}-\psi_{\mathrm{ry0,1}}\psi_{\mathrm{sx0,1}})+\frac{3p_2K_{\mathrm{r2}}}{2L_{\mathrm{s2}}'(J_1+J_2)}(\psi_{\mathrm{rx0,2}}\psi_{\mathrm{sy0,2}}-\psi_{\mathrm{ry0,2}}\psi_{\mathrm{sx0,2}})$$

$$N = \frac{3p_1K_{\mathrm{r1}}}{2L_{\mathrm{s1}}'J_1}(\psi_{\mathrm{rx0,1}}\ \psi_{\mathrm{sy0,1}} - \psi_{\mathrm{ry0,1}}\ \psi_{\mathrm{sx0,1}}) - \frac{3p_2K_{\mathrm{r2}}}{2L_{\mathrm{s2}}'J_2}(\psi_{\mathrm{rx0,2}}\ \psi_{\mathrm{sy0,2}} - \psi_{\mathrm{ry0,2}}\ \psi_{\mathrm{sx0,2}})$$

4.4 Stability Analysis

The stability of the system can be studied by studying the eigenvalues of characteristic matrix $\mathbf{A}$. The eigenvalues are typically in the form: $\lambda_i = \alpha_i + \mathrm{j}\omega_i$. The system is stable if the real parts of the eigenvalues are negative. If any one of the real parts is positive then the system renders unstable, and with zero real part the system sustain un-damped oscillations, however this requires very careful investigation.

4.5 Analytical Model

The analytical model for obtaining the transfer function of the system can be obtained by using Eq. (4.29) and Eq. (4.30). The small change in the stator voltage can be neglected; practically stator voltage stays the same. Taking Laplace transform of system of Eq. (4.30) results

$$\begin{cases} s\Delta\tilde{\psi}_{\mathrm{sx}} = -\dfrac{R_{\mathrm{s}}}{L_{\mathrm{s}}'}\Delta\tilde{\psi}_{\mathrm{sx}} + \omega_{\mathrm{k}}\Delta\tilde{\psi}_{\mathrm{sy}} + K_{\mathrm{r}}\dfrac{R_{\mathrm{s}}}{L_{\mathrm{s}}'}\Delta\tilde{\psi}_{\mathrm{rx}} \\ s\Delta\tilde{\psi}_{\mathrm{sy}} = -\omega_{\mathrm{k}}\Delta\tilde{\psi}_{\mathrm{sx}} - \dfrac{R_{\mathrm{s}}}{L_{\mathrm{s}}'}\Delta\tilde{\psi}_{\mathrm{sy}} + K_{\mathrm{r}}\dfrac{R_{\mathrm{s}}}{L_{\mathrm{s}}'}\Delta\tilde{\psi}_{\mathrm{ry}} \\ s\Delta\tilde{\psi}_{\mathrm{rx}} = K_{\mathrm{s}}\dfrac{R_{\mathrm{r}}}{L_{\mathrm{r}}'}\Delta\tilde{\psi}_{\mathrm{sx}} - \dfrac{R_{\mathrm{r}}}{L_{\mathrm{r}}'}\Delta\tilde{\psi}_{\mathrm{rx}} + (\omega_{\mathrm{k}}-\omega_0)\Delta\tilde{\psi}_{\mathrm{ry}} - s\Delta\tilde{\theta}\psi_{\mathrm{ry0}} \\ s\Delta\tilde{\psi}_{\mathrm{ry}} = K_{\mathrm{s}}\dfrac{R_{\mathrm{r}}}{L_{\mathrm{r}}'}\Delta\tilde{\psi}_{\mathrm{sy}} - (\omega_{\mathrm{k}}-\omega_0)\Delta\tilde{\psi}_{\mathrm{rx}} - \dfrac{R_{\mathrm{r}}}{L_{\mathrm{r}}'}\Delta\tilde{\psi}_{\mathrm{ry}} + s\Delta\tilde{\theta}\psi_{\mathrm{rx0}} \end{cases} \tag{4.35}$$

This can be further simplified into

$$\begin{cases} 0 = -\left(s + \dfrac{R_{\mathrm{s}}}{L_{\mathrm{s}}'}\right)\Delta\tilde{\psi}_{\mathrm{sx}} + \omega_{\mathrm{k}}\Delta\tilde{\psi}_{\mathrm{sy}} + K_{\mathrm{r}}\dfrac{R_{\mathrm{s}}}{L_{\mathrm{s}}'}\Delta\tilde{\psi}_{\mathrm{rx}} \\ 0 = -\omega_{\mathrm{k}}\Delta\tilde{\psi}_{\mathrm{sx}} - \left(s + \dfrac{R_{\mathrm{s}}}{L_{\mathrm{s}}'}\right)\Delta\tilde{\psi}_{\mathrm{sy}} + K_{\mathrm{r}}\dfrac{R_{\mathrm{s}}}{L_{\mathrm{s}}'}\Delta\tilde{\psi}_{\mathrm{ry}} \\ s\Delta\tilde{\theta}\psi_{\mathrm{ry0}} = K_{\mathrm{s}}\dfrac{R_{\mathrm{r}}}{L_{\mathrm{r}}'}\Delta\tilde{\psi}_{\mathrm{sx}} - \left(s + \dfrac{R_{\mathrm{r}}}{L_{\mathrm{r}}'}\right)\Delta\tilde{\psi}_{\mathrm{rx}} + (\omega_{\mathrm{k}}-\omega_0)\Delta\tilde{\psi}_{\mathrm{ry}} \\ -s\Delta\tilde{\theta}\psi_{\mathrm{rx0}} = K_{\mathrm{s}}\dfrac{R_{\mathrm{r}}}{L_{\mathrm{r}}'}\Delta\tilde{\psi}_{\mathrm{sy}} - (\omega_{\mathrm{k}}-\omega_0)\Delta\tilde{\psi}_{\mathrm{rx}} - \left(s + \dfrac{R_{\mathrm{r}}}{L_{\mathrm{r}}'}\right)\Delta\tilde{\psi}_{\mathrm{ry}} \end{cases} \tag{4.36}$$

In matrix form

$$\Delta\tilde{\theta}\begin{bmatrix}0\\0\\s\psi_{\mathrm{ry0}}\\-s\psi_{\mathrm{rx0}}\end{bmatrix}=\begin{bmatrix}-s-\frac{R_\mathrm{s}}{L'_\mathrm{s}} & \omega_\mathrm{k} & K_\mathrm{r}\frac{R_\mathrm{s}}{L'_\mathrm{s}} & 0\\ -\omega_\mathrm{k} & -s-\frac{R_\mathrm{s}}{L'_\mathrm{s}} & 0 & K_\mathrm{r}\frac{R_\mathrm{s}}{L'_\mathrm{s}}\\ K_\mathrm{s}\frac{R_\mathrm{r}}{L'_\mathrm{r}} & 0 & -s-\frac{R_\mathrm{r}}{L'_\mathrm{r}} & \omega_\mathrm{k}-\omega_0\\ 0 & K_\mathrm{s}\frac{R_\mathrm{r}}{L'_\mathrm{r}} & \omega_\mathrm{k}-\omega_0 & -s-\frac{R_\mathrm{r}}{L'_\mathrm{r}}\end{bmatrix}\begin{bmatrix}\Delta\tilde{\psi}_{\mathrm{sx}}\\ \Delta\tilde{\psi}_{\mathrm{sy}}\\ \Delta\tilde{\psi}_{\mathrm{rx}}\\ \Delta\tilde{\psi}_{\mathrm{ry}}\end{bmatrix} \tag{4.37}$$

Finally, the matrix equation can be written in short notation as

$$\begin{aligned}\Delta\tilde{\theta}\mathbf{b}&=\mathbf{a}\Delta\tilde{\psi}\\ \mathbf{b}&=\mathbf{a}\frac{\Delta\tilde{\psi}}{\Delta\tilde{\theta}}\\ \mathbf{a}^{-1}\mathbf{b}&=\frac{\Delta\tilde{\psi}}{\Delta\tilde{\theta}}\end{aligned} \tag{4.38}$$

Similarly, the torque Eq. (4.29) can be written in matrix form as

$$\Delta\tilde{\tau}_\mathrm{e}=\frac{3}{2}p\frac{K_\mathrm{r}}{L'_\mathrm{s}}\begin{bmatrix}-\psi_{\mathrm{ry0}} & \psi_{\mathrm{rx0}} & \psi_{\mathrm{sy0}} & -\psi_{\mathrm{sx0}}\end{bmatrix}\begin{bmatrix}\Delta\tilde{\psi}_{\mathrm{sx}}\\ \Delta\tilde{\psi}_{\mathrm{sy}}\\ \Delta\tilde{\psi}_{\mathrm{rx}}\\ \Delta\tilde{\psi}_{\mathrm{ry}}\end{bmatrix}$$

The matrix equation can be written using short notation as

$$\Delta\tilde{\tau}_\mathrm{e}=\mathbf{c}\Delta\tilde{\psi} \tag{4.39}$$

Dividing Eq. (4.39) by $\Delta\tilde{\theta}$ and using Eq. (4.38) we get

$$\frac{\Delta\tilde{\tau}_\mathrm{e}}{\Delta\tilde{\theta}}=\mathbf{c}\frac{\Delta\tilde{\psi}}{\Delta\tilde{\theta}} \tag{4.40}$$

$$\frac{\Delta\tilde{\tau}_\mathrm{e}}{\Delta\tilde{\theta}}=\mathbf{c}\mathbf{a}^{-1}\mathbf{b} \tag{4.41}$$

Impulse Response Test

The impulse response can be performed to get the frequency response function. An impulse covers a wide range of non-zero frequency content. So, it becomes quite simple to see the frequency response at desired frequency with just one simulation. The impulse excitation that can be applied to the rotor position angle is defined as follows

$$\Delta\Theta_\mathrm{r}(t)=\begin{cases}\alpha_\mathrm{rel}\tau_\mathrm{p}\sin(2\pi f_\mathrm{d}), & t_1\le t\le t_1+t_\mathrm{d}\\ 0, & \text{otherwise}\end{cases} \tag{4.42}$$

where, α_{rel} is the relative amplitude, τ_{p} is the pole pitch, t_1 is the starting time of impulse, and t_d is the duration of the impulse. The frequency f_d is chosen such that the impulse is a half sine wave. The frequency content of above impulse can be adjusted by taking proper length. Smaller the length higher is the frequency content. An example could be if the length is 10 ms then the non-zero frequency content could be upto 200 Hz [17].

The impulse defined by Eq. (4.42) is applied to the position angle of the rotor, θ_{r}. The steady-state torque, τ_{e0}, and rotor position angle, θ_{r0}, is then eliminated by subtracting from the torque and rotor position angle obtained from impulse response. The result obtained are then impulse to the angle, $\Delta\theta_{\text{r}}$, and the response of the electro-magnetic torque, $\Delta\tau_{\text{e}}$, which are then converted to the frequency domain using DFT. The FRF is then obtained by taking the ratio of $\Delta\tau_{\text{e}}$ and $\Delta\theta_{\text{r}}$. The FRF shown in Fig. 1.1 was obtained using the above mentioned numerical impulse method by FEA.

5 Measurement Results

Diagram of the complete system and description of the components are mentioned below

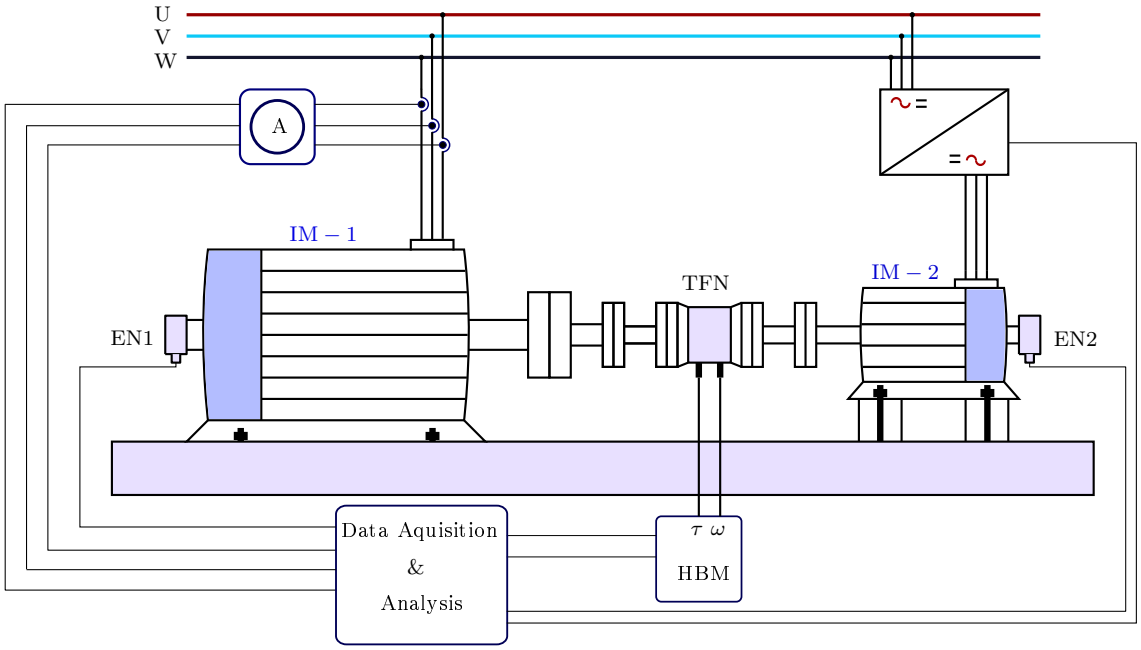

Figure 5.1: Experimental set-up layout

- U,V,W : Grid supply voltage
- A : Line current measurement unit
- IM-1 : 37 kW Cage induction machine
- IM-2 : 4 kW Cage induction machine
- EN1, EN2 : Encoder[3]
- TFN : Torque transducer[4]
- HBM : Torque amplifier

Hall Effect sensors are used to measure the line current. The optical encoders shown in the layout of Fig. 5.1 are of optical type with 1024 pulse per revolution (ppr) as an output. The torque transducer used in the set-up has a rated nominal torque of 200 Nm. Also, the coupling accessories fitted with torque transducer is characterised of having torsional stiffness equal to 31.5 kNm/rad. An additional coupling can be seen between the flexible coupling and shaft of 37 kW induction machine. This coupling somehow is large and could be modelled as the lumped inertia.

[3]Optical Encoders are of Leine & Linde type whose technical specifications can be found at http://www.leinelinde.se

[4]Torque transducer is of T30FNA type from Hottinger Baldwin Messtechnik (HBM) whose technical specification can be found at http://www.hbm.com

5.1 Simulation Results

The main simulation result has been mentioned in the objective (Fig. 1.1). Furthermore, the detailed explanation of frequency response analysis has been explained in previous chapters. Now, the result from the stability analysis and hence small signal model will be mentioned. In order to perform the simulations, machine parameters[5] estimated using FEA (finite element analysis) were taken into consideration. The machine parameters are mentioned in Table. 5.1.

Table 5.1: Machine parameters

Parameter	**4 kW Machine**	**37 kW Machine**
u	380 V	380 V
f	50 Hz	50 Hz
RPM	1425	1470
p	2	2
R_{s}	1.39 Ω	0.08005 Ω
R_{r}	1.11 Ω	0.06077 Ω
X_{m}	44.82 Ω	7.84452 Ω
$X_{\mathrm{s}\sigma}$	2.02 Ω	0.24497 Ω
$X_{\mathrm{r}\sigma}$	1.91 Ω	0.50256 Ω
J	0.015 kg · m^2	0.256 kg · m^2

5.1.1 Study of Eigenvalues

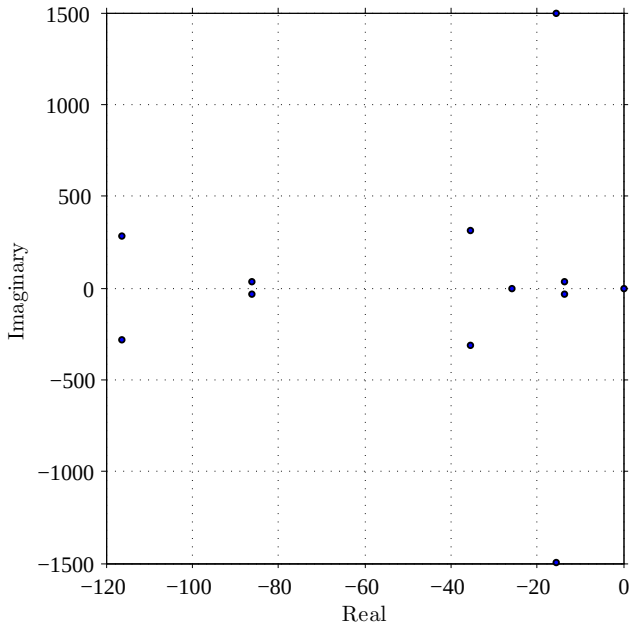

Figure 5.2: Eigenvalues of the system

[5]Available from Department of Electrical Engineering & Automation, Aalto University

Fig. 5.2 is the simulation result from the small-signal model which represents the eigenvalues of the characteristic matrix **A**. From Fig. 5.2 it is clear that real part of eigenvalues lies in negative half-plane, except for one real part, which lies at the origin. The zero real part of eigenvalue was expected due to rigid body mode. There is no damping as well as oscillation in this mode. Hence, relying on this result we can firmly conclude that the system is stable when run at no-load condition.

5.1.2 Direct Simulation and Result from Small-signal Model

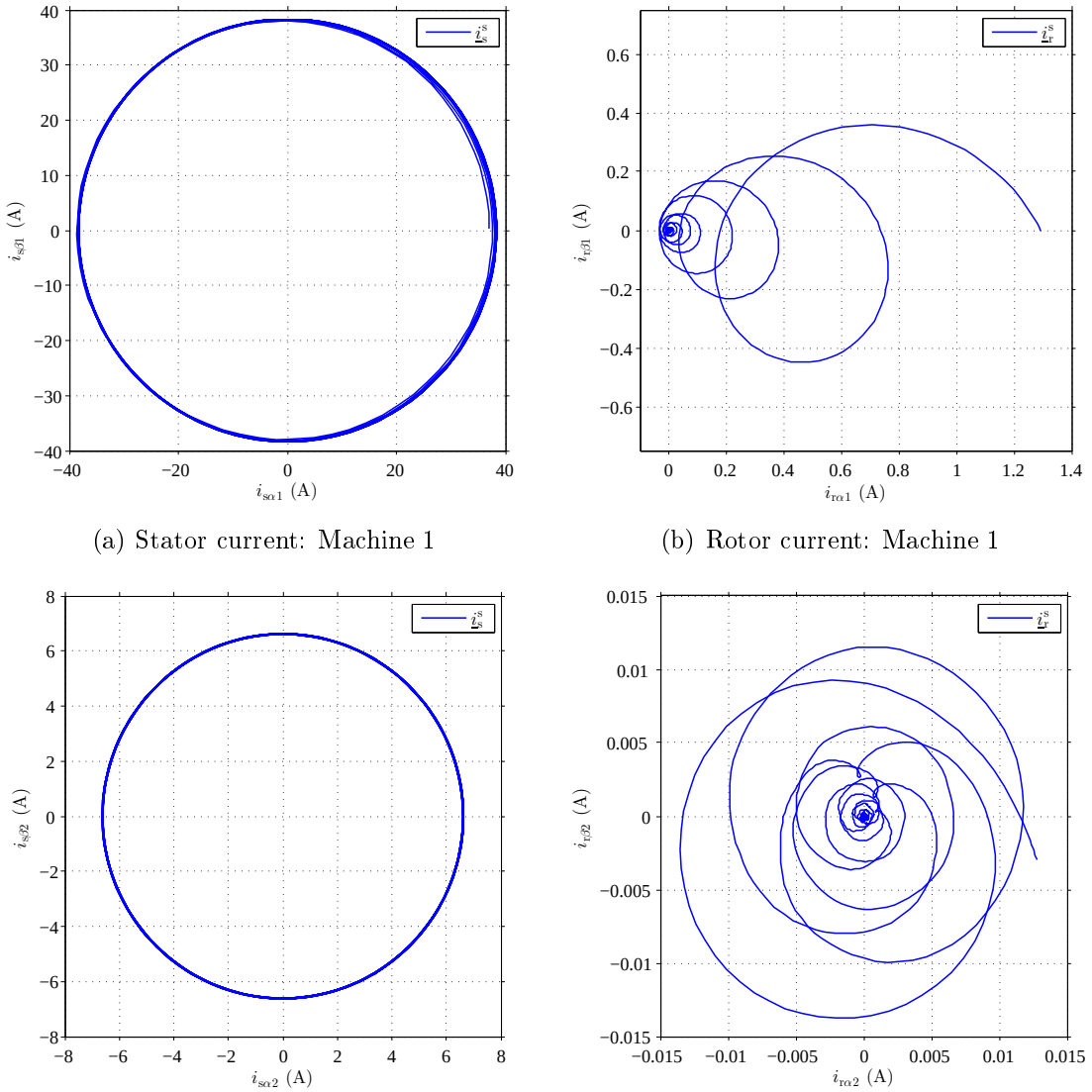

(a) Stator current: Machine 1

(b) Rotor current: Machine 1

(c) Stator current: Machine 2

(d) Rotor current: Machine 2

Figure 5.3: Current space vectors obtained from direct simulation

Fig. 5.3 is the result obtained from direct simulation of Eq. (3.1)–Eq. (3.2) and Eq. (4.8)–Eq. (4.10). Initial conditions from steady-state values were taken into

consideration. The result depicts that there is extremely small oscillation, due to which the lines are slightly thick. In overall, the system seems to be stable. Also, it could be noticed that the rotor current is of very small amplitude at no-load condition. The oscillation in rotor current decays away quickly to zero. The no-load peak value of current in the stator winding of 37 kW machine was calculated to be 38.35 A, and that of 4 kW machine was calculated to be 6.62 A. The simulations have also given almost the same values.

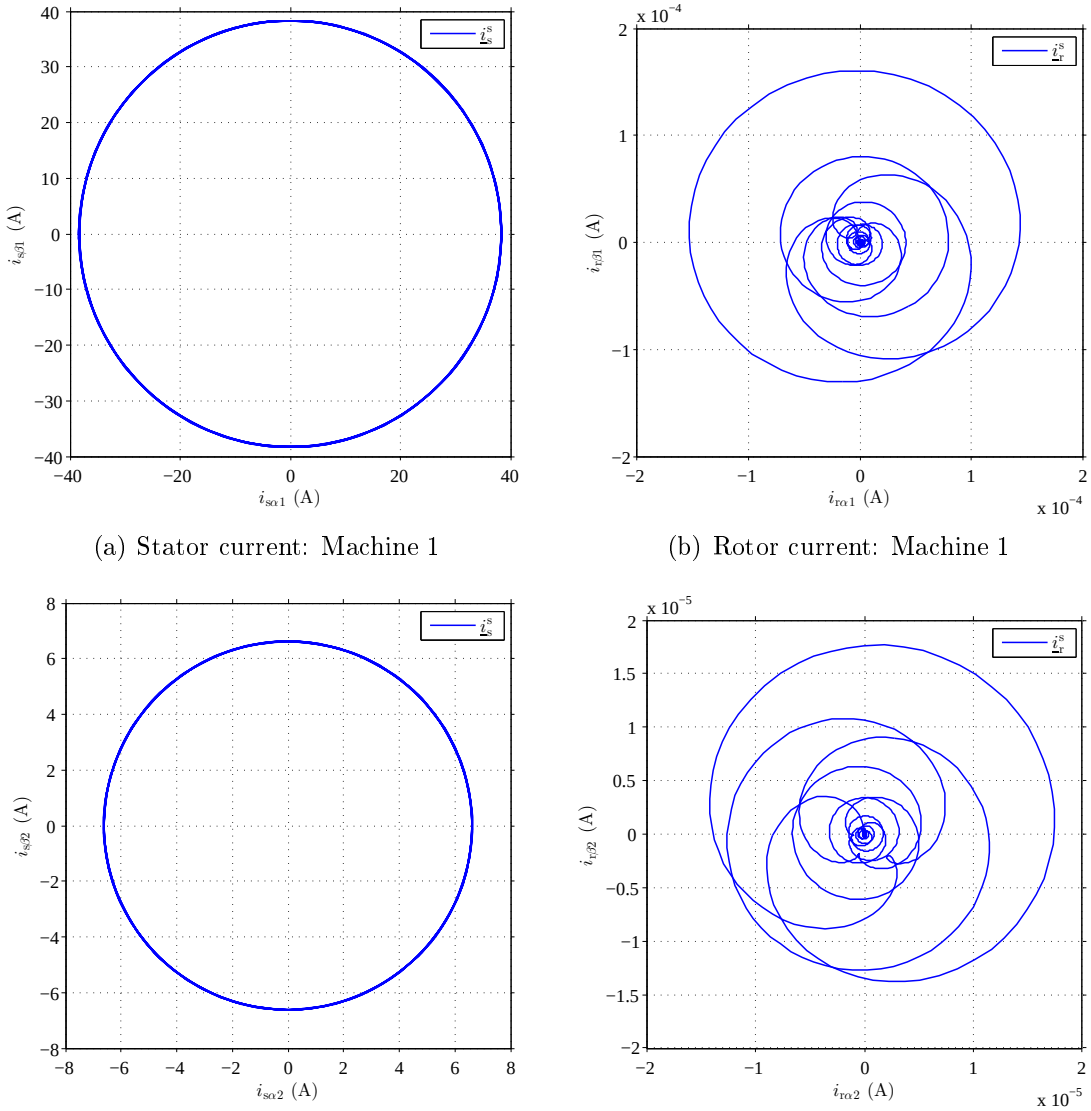

(a) Stator current: Machine 1

(b) Rotor current: Machine 1

(c) Stator current: Machine 2

(d) Rotor current: Machine 2

Figure 5.4: Current space vectors obtained from small-signal model

The simulation result from small-signal model is shown in Fig. 5.4. Current space-vectors from steady-state condition were added to the result for comparison purpose. From the eigenvalue study, it was of no surprise that the small-signal model will result in quite stable rotating space vectors. However, there are some

small variations which can be seen in rotor current, and eventually they attenuate to zero. For small-signal analysis initial values of rotor currents were assumed to be zero.

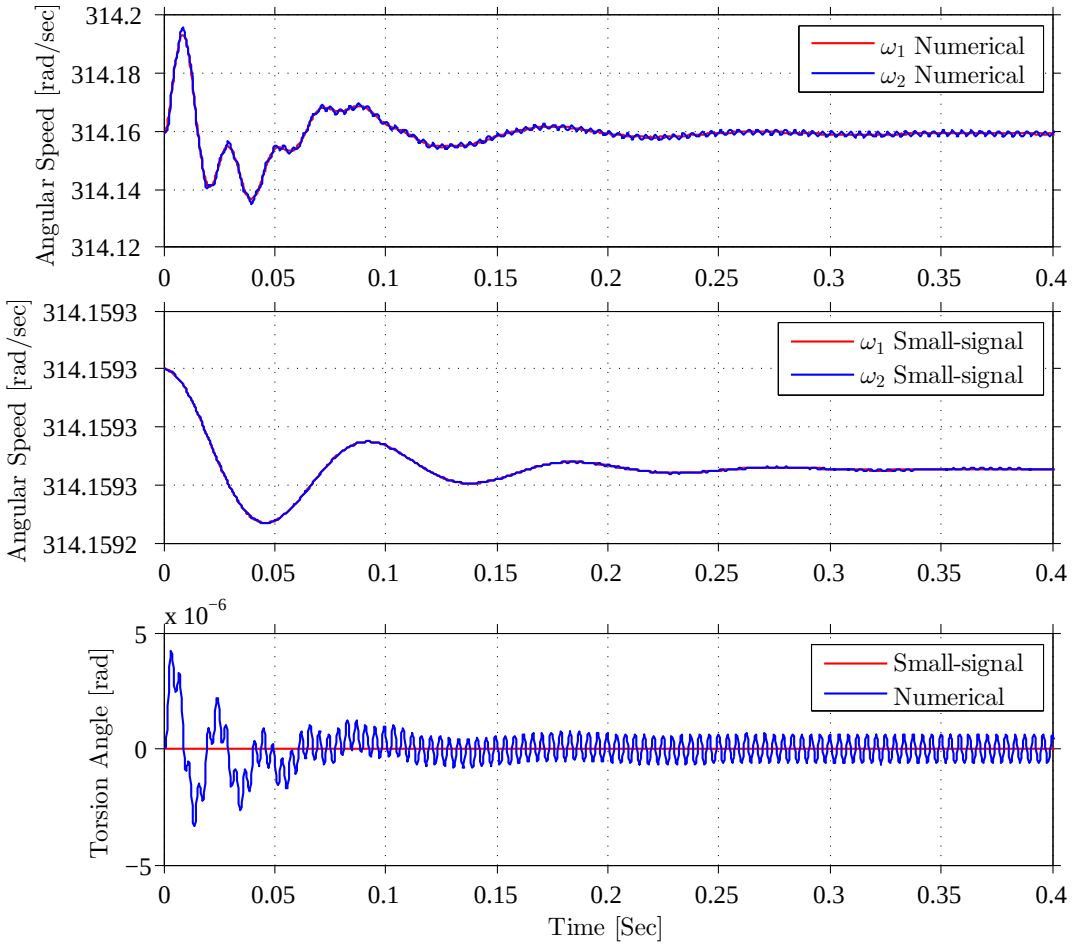

Figure 5.5: Angular speed of cage-induction machines at no load condition

Fig. 5.5 compares the result from direct simulation and small-signal model, between angular speed and torsion angle. Direct simulation shows small oscillation in both rotor speed and torsion angle. The oscillation in angular speed of the machine with small inertia seems higher compared to machine with larger inertia, and hence this confirms the relation obtained in Eq. (3.16b). However, the oscillations are not so visible from small-signal model. Actually, the oscillation in either angular speed or torsion angle is quite small, which can also be seen from the y–axis values. The figures are highly zoomed in-order to see the difference between two simulations.

5.1.3 Verification of Analytical Model

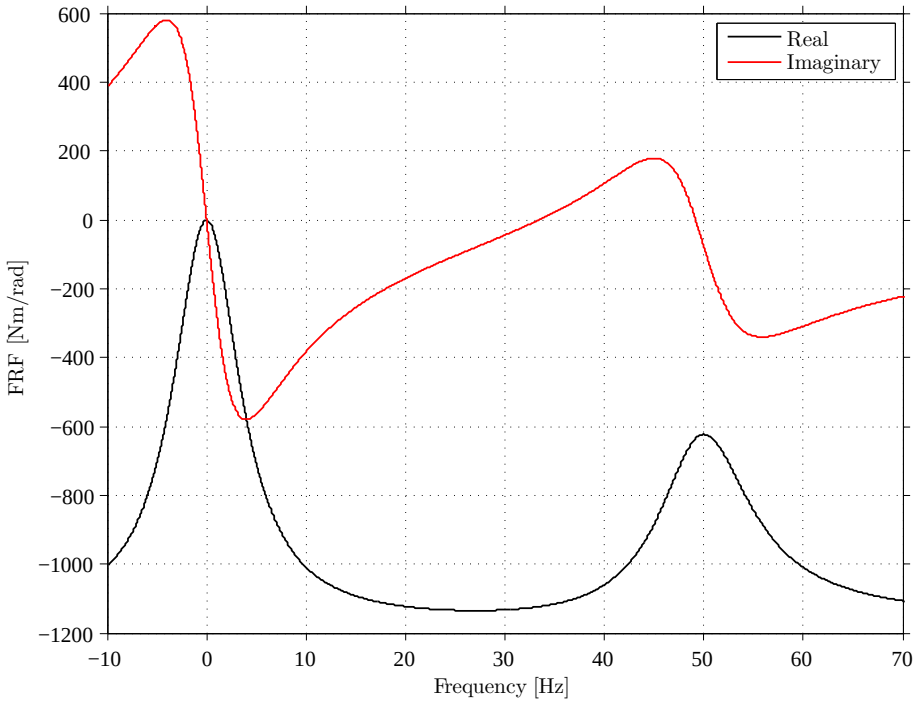

Figure 5.6: FRF of 37 kW cage-induction machine at no load condition

The analytical model formulated in Sub-Section 4.5 was simulated using Matlab®. Eq. (4.41) presents the actual frequency response function from rotor position angle to electro-magnetic torque of cage-induction machine. The simulation result shown in Fig. 5.6 represents the FRF of 37 kW cage-induction machine at no load condition. In Fig. 5.6, the imaginary part of FRF represents the electromagnetic damping while the real part of FRF represents electromagnetic stiffness. To no surprise the result shown in Fig. 5.6 resembles with the result of Fig 1.1. However, the difference among these two simulation result can be seen in the width of negative damping and amplitude. If we take frequency range from 0 Hz – 100 Hz then the region of negative damping is much wider (34 Hz – 49 Hz) in case of result shown in Fig. 5.6, but in the case of Fig. 1.1, the negative damping range is slightly narrow (40 Hz – 49 Hz). The result of Fig. 5.6 is highly sensitive to variation in resistance and inductance. Both stator resistance and leakage inductance varies from no load to rated operating condition of an induction machine. The FRF results with different stator resistance, load conditions and skin effect has been briefly explained by Repo *et al.* [17]. Repo *et al.* have computed the FRF of 37 kW cage-induction machine at different load conditions, and found that the increase in load widens the frequency range and increases the amplitude of negative damping.

Clearly, the presence of negative damping near frequency region close to synchronous speed is evident from the simulation results. The parameters used to obtain the result of Fig. 5.6 is mentioned in Table 5.1 and Table A.1 (Appendix A).

5.2 Laboratory Results

5.2.1 Three Mass System

The actual system layout is shown in Fig. 5.1. The actual system seems somehow complicated and resembles three mass systems. This is essentially due to presence of noticeable coupling between the shaft of larger machine, and torque transducer. Additional coupling has considerable mass and measurements were done to sort out the mass moment of inertia. The following equations were used for calculating the mass moment of inertia of additional coupling

$$J = \frac{MR^2}{2} \tag{5.1}$$

where, M is the mass of the object, and R is the radius of gyration. In case of solid cylinder R is taken to be the actual radius. The mass of the object can be calculated using

$$M = V\rho_{\text{Fe}} = \frac{\pi D^2 l}{4}\rho_{\text{Fe}} \tag{5.2}$$

where, D is the diameter of the cylinder, l is the length of cylinder, and ρ_{Fe} represents the specific density of the iron. The stiffness of the shaft section between masses were calculated using Eq. (3.18). The lumped three inertia model is shown in Fig. 5.7.

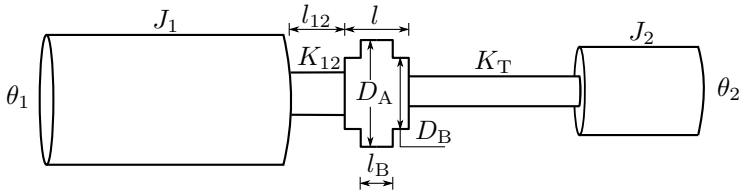

Figure 5.7: Lumped model for three mass system

Table 5.2: Parameters for three mass system

Parameter	Value
D_{A}	0.199 m
D_{B}	0.114 m
l	0.0895 m
l_{B}	0.0465 m
l_{12}	0.085 m
G	79.3 GPa
ρ_{Fe}	7860 kg/m^3
K_{12}	410096 Nm/rad
K_{T}	31500 Nm/rad
J_1	0.256 kgm^2
J_2	0.015 kgm^2
J_3	0.0581 kgm^2

The natural frequencies and the associated mode shapes for the lumped model shown in Fig. 5.7 were calculated using Eq. (3.14). The results are tabulated below

Table 5.3: Natual frequencies and associated modes

Natural Frequency	$f_1 = 0$Hz	$f_2 = 228.5$Hz	$f_3 = 483.79$Hz
Eigen Vectors	$\phi_1 = \begin{Bmatrix} -0.5774 \\ -0.5774 \\ -0.5774 \end{Bmatrix}$	$\phi_2 = \begin{Bmatrix} -0.0625 \\ 0.0180 \\ 0.9979 \end{Bmatrix}$	$\phi_3 = \begin{Bmatrix} -0.1972 \\ 0.9405 \\ -0.2766 \end{Bmatrix}$

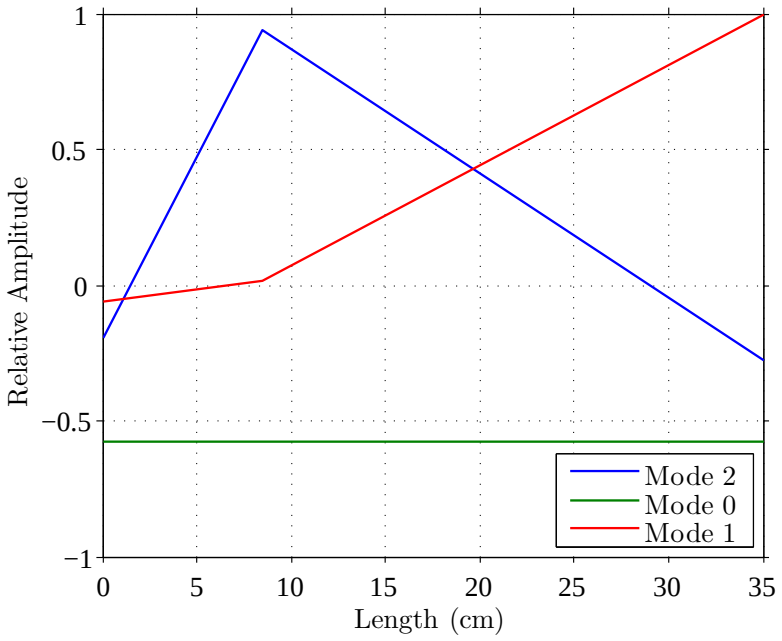

Figure 5.8: Mode shapes for three mass system

The natural frequencies obtained for both mode 1 and mode 2 are above frequency range of 0 Hz – 100 Hz. Also, there is no coincidence of the natural frequencies with excitation near synchronous speed. However, interference points exist near 1200, 1300, 1650 rpm for fundamental modal natural frequency, and this is somehow within the frequency range 30–60 Hz. Although, this is highly approximated result, we can still proceed further. The system will always be operated near synchronous speed so there isn't any interference near synchronous speed. But, the superimposed harmonic excitations are starting from 40 Hz upto 50 Hz, which could lead to resonance. Previously, the mechanical model was assumed to be two mass systems, and mechanical natural frequency of lumped two mass systems was calculated to be 237.3 Hz. The small-signal analysis is all based on this assumption. The natural frequencies with both two mass approximations and three mass approximations are shown in Fig. 3.4, as solid black lines. Although, laboratory set-up resembles three inertia model rather than two inertia model, the first modal natural frequency has not changed drastically.

5.2.2 Torque and Rotation Angle measurement

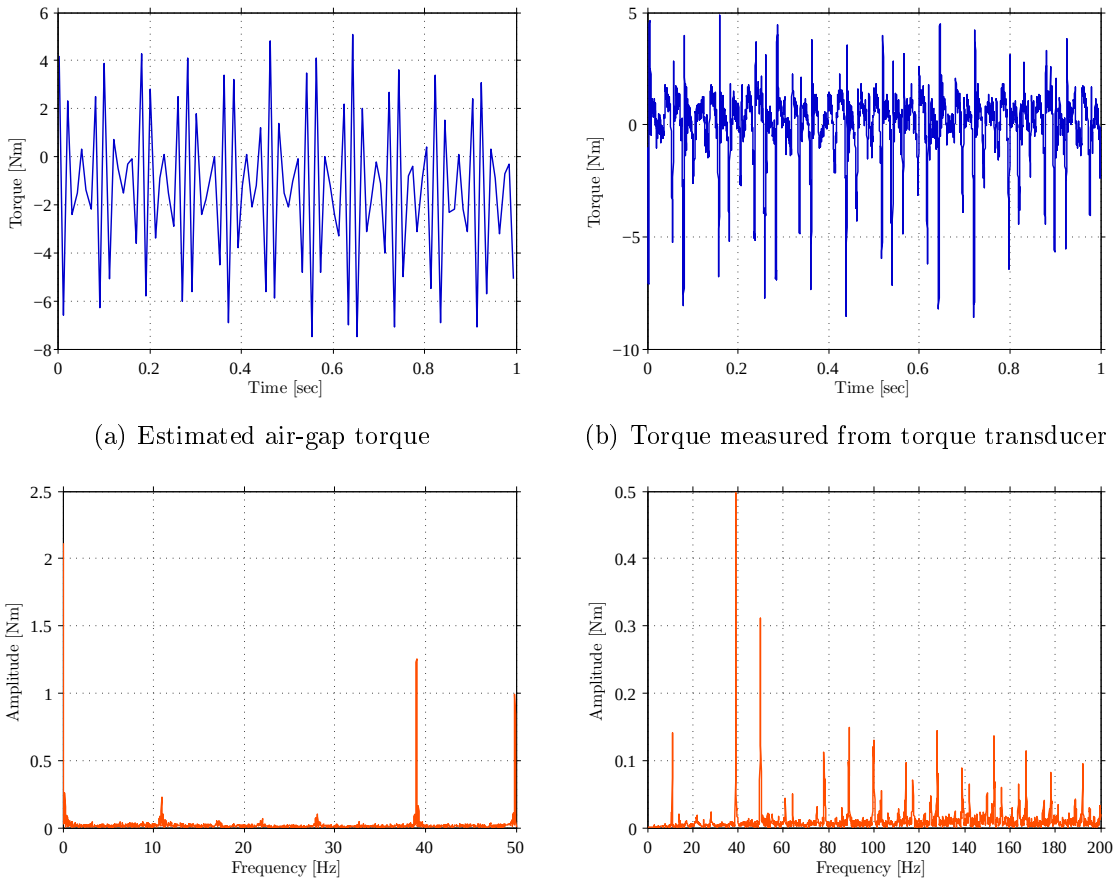

(a) Estimated air-gap torque

(b) Torque measured from torque transducer

(c) Amplitude spectrum of air-gap torque

(d) Amplitude spectrum of shaft-end torque

Figure 5.9: Torque measurement at 39 Hz harmonic excitation

Fig. 5.9(a) represents the estimated air-gap torque of 4 kW machine when excitation amplitude was fixed at 5 percent of rated torque of the machine, and frequency of excitation at 39 Hz. The sampling frequency was fixed at 100 Hz. A perfect sinusoid was supposed to be the outcome, but it seems quite distorted. Fig. 5.9(c) is the discrete Fourier transform (DFT) of the estimated air-gap torque, and to no surprise the fundamental harmonic is at 39 Hz. Due to sampling frequency of 100 Hz it was not possible to see higher order harmonics in the estimated air-gap torque using FFT algorithm in Matlab®. Similarly, Fig. 5.9(b) represents the measurement result from torque transducer. Measurement result from the torque transducer represents the shaft-end torque. The sampling frequency in this case has been fixed at 10,000 Hz. The shaft-end torque should in ideal case follow the excitation torque according to Eq. (3.21), and it does also in this case. The amplitude of the shaft-end torque seems quite near to the amplitude of the estimated air-gap torque with some scaling. To see the frequency components, a discrete Fourier transform has been performed and result is shown in Fig. 5.9(d). The component at the excitation frequency seems to

be the largest harmonic, and higher order harmonics at multiples of 39 Hz can also be seen. Also, component at line frequency and twice line frequency are present as expected.

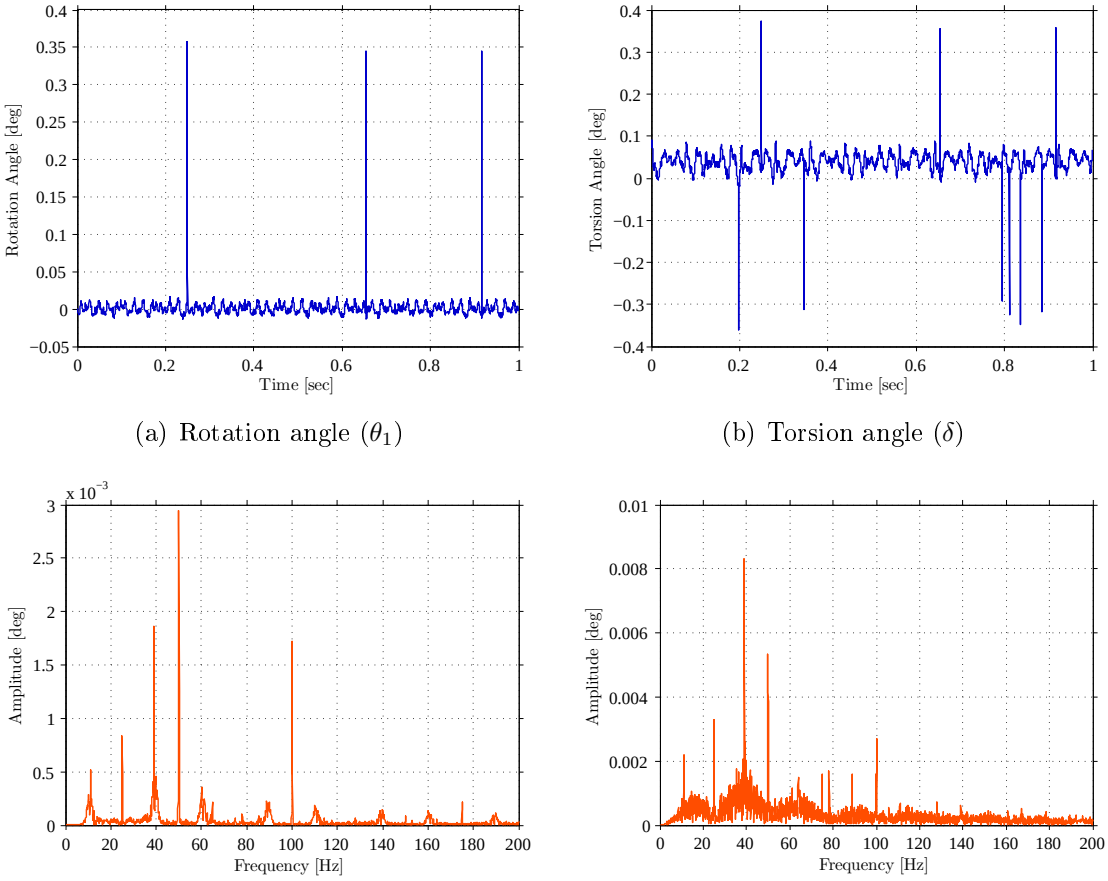

(a) Rotation angle (θ_1)

(b) Torsion angle (δ)

(c) Amplitude spectrum of (θ_1)

(d) Amplitude spectrum of (δ)

Figure 5.10: Rotation angle measurement at 39 Hz harmonic excitation

Fig. 5.10(a) represents filtered rotation angle measurement taken during 39 Hz harmonic excitation. The rotation angle was obtained using encoder connected to non-drive end of 37 kW induction machine. The sampling frequency was fixed at 10,000 Hz. Similarly, filtered value of rotation angle was also measured from second encoder, which was attached to non-drive end of 4 kW machine. Now using difference of two rotation angle measurement, torsion angle was obtained as shown in Fig. 5.10(b). A DFT of rotation angle is shown in Fig. 5.10(c), and Fig. 5.10(d) is a Fourier transform of torsion angle. The amplitude spectrum of rotation angle has components at rotational speed i.e. 25 Hz, component at 39 Hz excitation frequency, line frequency component, and twice line frequency component. These components were all expected except for a small component at 10 Hz. Also, amplitude at 39 Hz component was expected to be the largest, which isn't the case now.

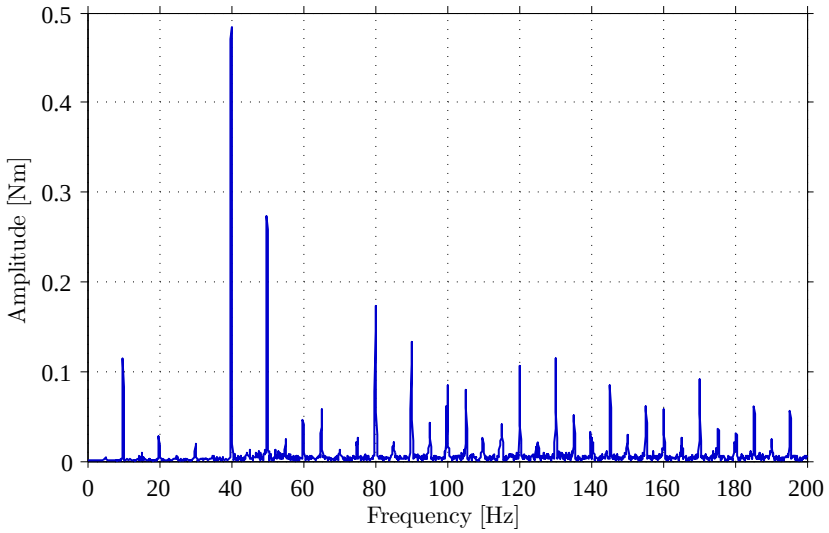

Figure 5.11: Amplitude spectrum of shaft-end torque at 40 Hz excitation

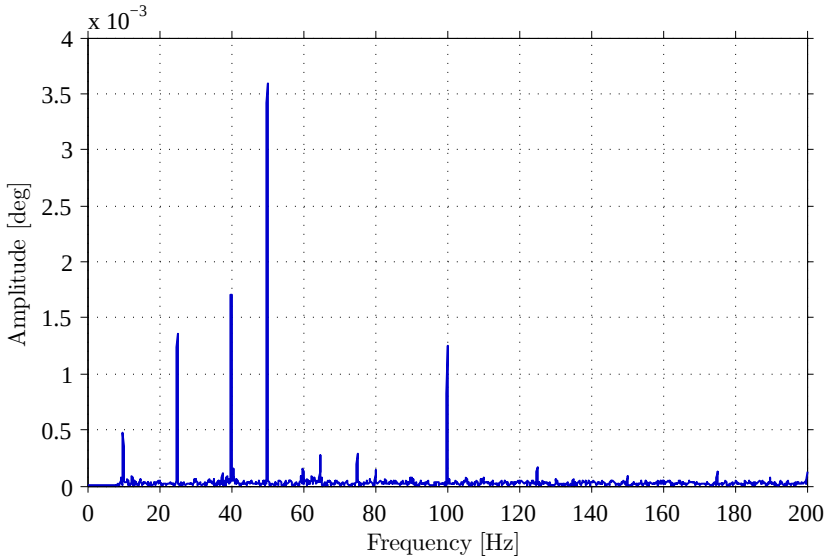

Figure 5.12: Amplitude spectrum of filtered value of rotation angle

The above Fig. 5.11 represents the amplitude spectrum of measured shaft-end torque when harmonic excitation at 40 Hz was provided. The amplitude spectrum was obtained using discreet Fourier transform algorithm in Matlab®. The excitation torque's peak amplitude was fixed at 5 percent of 26 Nm. In the measured torque it was obvious that amplitude corresponding to 40 Hz component would be the largest and also the fundamental harmonic. However, component at line frequency and twice line frequency are also present. Harmonics at multiples of excitation frequency can also be seen in the amplitude spectrum of Fig. 5.11. A small amplitude at 10 Hz looks somehow strange but could be possibly due to drive excitation component

$k = 6$, $m = -6$. Components at 60 Hz could also be possibly due to drive excitation component $k = 6$, $m = -6$, similarly a small component at 140 Hz could be due to $k = 6$, $m = -2$, this can be referred to Campbell diagram of Fig. 3.4. Some components are quite difficult to explain with reasonable cause for their presence, for example 90 Hz component.

Fig. 5.12 represents the amplitude spectrum of filtered value of rotation angle. Rotation angle linearly rises, but the encoder signals are in the form of pulses which are counted per revolution of the shaft. The counter signals are sawtooth signal which rises linearly from 0° upto 360° per revolution of the shaft. The frequency of this sawtooth wave was 25 Hz, that corresponds to 1500 rpm. The vibration superimposed in linearly rising rotation angle was filtered out, and Fig. 5.12 is the discrete Fourier transform of the filtered rotation angle. In the amplitude spectrum, components at 25 Hz, 40 Hz, 50 Hz and 100 Hz are most prominent while 50 Hz component have the largest amplitude. Also, 75 Hz component could possibly be a 3rd harmonics corresponding to 25 Hz rotational speed component. In the same fashion measurements were done when no excitations were provided, and this was named steady-state measurements. The steady-state measurements are shown in Fig. 5.13.

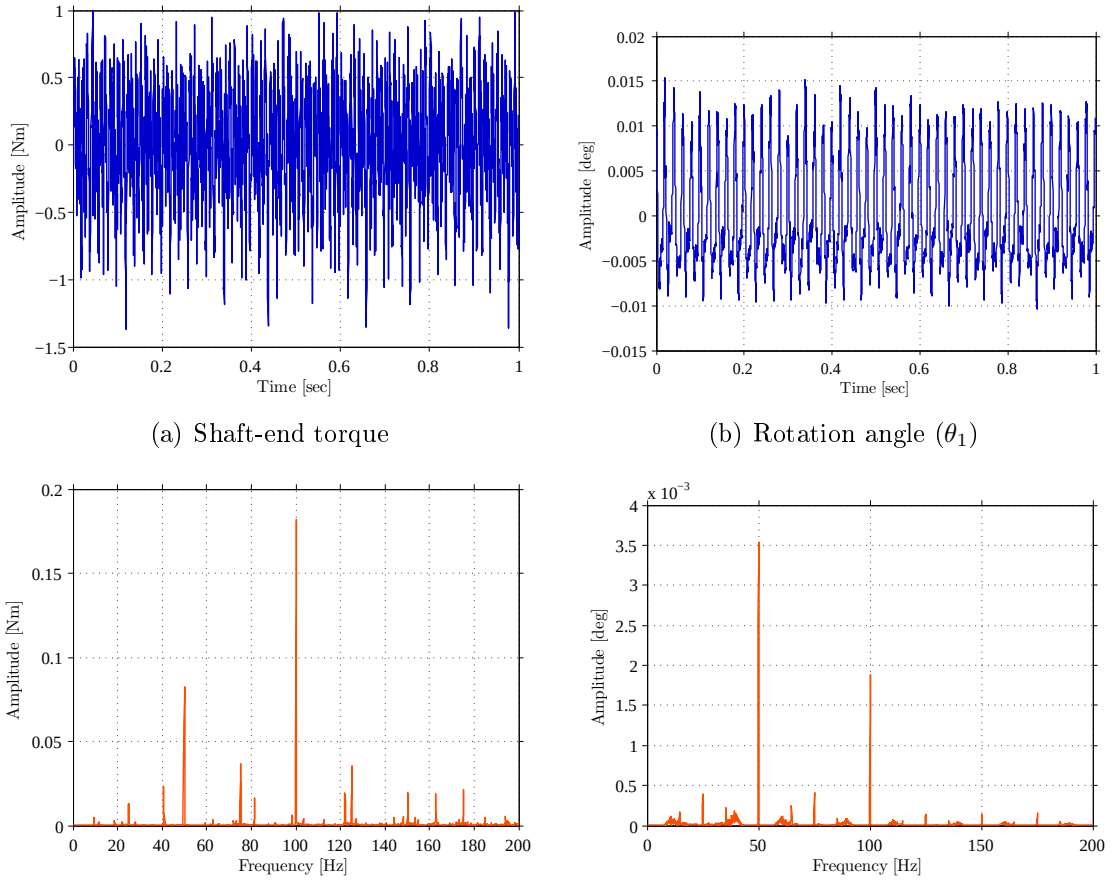

(a) Shaft-end torque

(b) Rotation angle (θ_1)

(c) Amplitude spectrum of torque

(d) Amplitude spectrum of (θ_1)

Figure 5.13: Steady-state measurement

5.2.3 Frequency Response Analysis

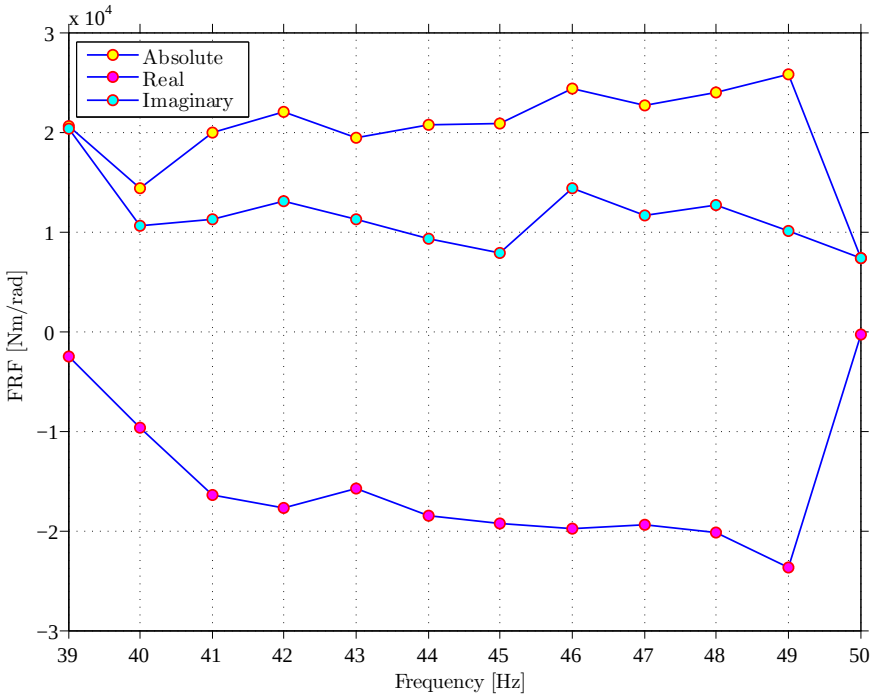

(a) FRF = $\frac{\Delta\tau_{\mathrm{e}}(\mathrm{j}\omega)}{\Delta\theta_{\mathrm{r}}(\mathrm{j}\omega)}$

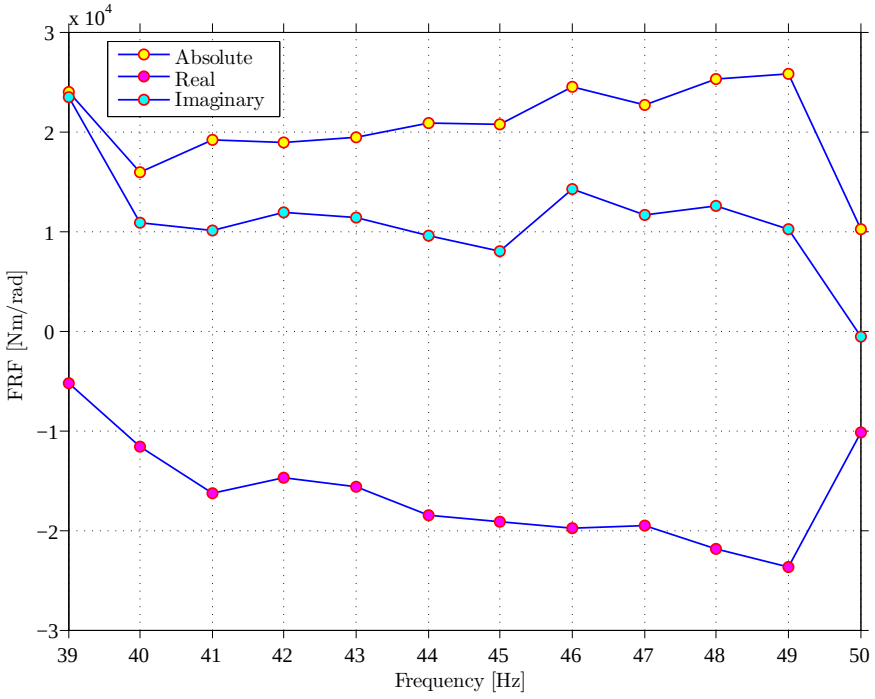

(b) FRF = $\frac{\tau_{\mathrm{e}}(\mathrm{j}\omega)}{\theta_{\mathrm{r}}(\mathrm{j}\omega)}$

Figure 5.14: Frequency Response Function

The measurement results obtained in Fig. 5.14(a) and Fig. 5.14(b) represent the frequency response function obtained by dividing torque component at particular frequency by the component of filtered rotation angle at that particular frequency. Fig. 5.14(a) essentially makes use of the small-signal model, where the steady-state measurement results are subtracted from the measurement results obtained while providing the excitation torque. Small signal torque ($\Delta\tau_e$) and small-signal rotation angle ($\Delta\theta_r$) were obtained by this method. For subtracting two measurement signals taken at different time instants, phase angle of the fundamental component of line current was taken into consideration. The line current measurements were done for both conditions, with excitation torque provided and without excitation torque provided. Further, a DFT was performed for measured line currents, and phase angle of the fundamental component was extracted and compared. The torque and rotation angle measured during excitation were then phase shifted by a value equal to difference in phase angle of the fundamental current components. The measurement signals during the excitation were always phase shifted to be aligned with the steady-state measurement signal. Finally, the phase shifted signals were inverse Fourier transformed and were used to subtract the steady-state signal in time domain. This is how the small-signal model was obtained.

After performing signal subtraction, a DFT is done for both small-signal torque and small-signal filtered rotation angle. Once the complex values in frequency domain were obtained, FRF was then formulated by extracting the needed frequency component, ranging from 39 Hz upto 50 Hz, with a resolution of 1 Hz. Finally, the frequency component of small-signal torque was divided by the same frequency component of small-signal rotation angle. The obtained results were then plotted as shown in Fig. 5.14(a). A second FRF was also obtained as shown in Fig. 5.14(b), but in this case no small-signal model was formulated, instead the needed frequency component of measured torque was directly divided by the same frequency component of the measured rotation angle taken during excitation. The assumption behind obtaining second FRF was that, no frequency component in the range 39 Hz – 50 Hz should be present in the steady-state signals. Nevertheless, this was not a strong argument, since frequency component at line frequency was always present. Also, this can be seen in steady-state measurements of Fig. 5.13(c) that line frequency component made an obvious presence. However, the second FRF still seems reasonable compared to small-signal FRF.

Comparison

i. Real Part of FRF
   The real part of FRF obtained from measurement result seems negative in both Fig. 5.14(a) and Fig. 5.14(b). This somehow resembles the simulation result of Fig. 1.1. If we take the simulation result of Fig. 1.1 then real part of FRF increases starting from 40 Hz upto 50 Hz, but measurement result doesn't have any close agreement with the kind of trend seen in simulation. But in case of measurement result, the real part starting from 39 Hz first decreases upto 49 Hz and then rises.

ii. Imaginary Part of FRF
The imaginary part of FRF obtained from measurement result is positive in both Fig. 5.14(a) and Fig. 5.14(b). This somehow resembles the simulation result of Fig. 1.1. Except for a point at 39 Hz, the measurement result is tending to have closer resemblance to the simulation result. In the simulation result, the values first rises starting from 40 Hz upto 45 Hz and then decreases towards negative, this is somehow true in case of measurement result, if we only considered results starting from 40 Hz. However, imaginary part in Fig. 5.14(a) remains all positive even at 50 Hz and only in Fig. 5.14(b) it seems that the results are getting closer towards negative side, eventually at 50 Hz.

iii. Absolute part of FRF
There is no plot of absolute value in simulation result of Fig. 1.1. It seems quite evident that absolute value of FRF should follow the real part of FRF, since this is the largest value. Imaginary part seems quite small in the frequency range of 40 Hz – 50 Hz, therefore real part dominates in absolute value curve. If we consider only 40 Hz upto 50 Hz range then the absolute value will be maximum at 40 Hz and gradually decrease, and finally attain minimum at 50 Hz. The measurement result does not follow such trend, since the values are somehow close to each other. Starting at 40 Hz, the absolute values slightly rises until it reaches its maximum at 49 Hz and then falls at 50 Hz.

6 Summary

A rigorous analysis of a drive system involving cage induction machine was performed. A study on possible excitation system was also performed and new kind of excitation system was proposed followed by its suitability and stability analysis. Analytical models were also developed to analyse the proposed system. The proposed exciter set-up was built with available components in the machine hall of Department of Electrical Engineering and Automation. With a successful testing, measurements were carried out for validating the simulation result. Three sets of measurements were done and only best one was considered for further analysis. Due to possibility of fine tuning the frequency converter for both peak amplitude of air-gap torque and excitation frequency, it was possible to obtain quick results. The results obtained somehow agree with the simulation result but still a lot of disagreement hovers. The result seems somehow compromised in accuracy compared to simulation result. The measurement result strongly support for an existence of possible negative electromagnetic damping within the frequency range of 40 Hz – 50 Hz. The mentioned frequency range is quite close to the operation range of induction machine. Also, a shift in natural frequency of drive system seems quite evident due to stiffening phenomena provided by the electro-magnetic system. This is a strong message to the scientific community that a much deeper study of effects related to electro-magnetic interaction must be done. This could be a needed concern to be addressed by the system designer as well. If the design consideration leads to a natural frequency obtained only by considering mechanical model, then it might lead to somehow a compromised design. If the natural frequency of a drive system has been fixed to a value lower than its operating speed, then a shift in the natural frequency due to the electro-magnetic system could bring the natural frequency near the operating speed, and this could affect the overall performance of the drive system. This is an open question that this master this work has been emphasizing from the start.

The compromised results obtained leave us with more possible option to fine tune the excitation system. Some of the possible improvement for a better result could be:

i. The estimated air-gap torque from the frequency converter was found to be non-sinusoidal, seems almost triangular. This has to be near to sinusoidal for perfect harmonic excitation. A triangular wave is superimposed of many sinusoids. This is undesirable and a possible cause of undesirable excitations. The control algorithm in the frequency converter needs more fine tuning.

ii. Both the cage-induction machines are supposed to run at no load, and on top of that a harmonic excitation was supposed to be superimposed. This somehow didn't happen due to problem in synchronizing smaller induction machine with the larger one. A possible alternative would be to run the small machine at loaded condition so that a harmonic component could be superimposed in the DC component of the air-gap torque.

iii. A careful view of the coupled system somehow deviates from its two mass model, which can be seen in Fig. B.1. A large coupling between the shafts of large induction machine with the second coupling accommodating torque transducer seems quite large, leading to a three mass system. Also, the shaft sections were not uniform and at one place smaller diameter shaft was used. The small section of shaft was found to be quite small and possibly could decrease the equivalent stiffness of the shaft system. Although it's not a big change but somehow a concern for approximating the system's natural frequency.

iv. The supporting frames of the encoders were bolted to the machine base. The whole base starts vibrating as the machine operates, and this causes vibration in the encoder as well. This might have led to undesirable oscillating frequency components in the measurement. A better approach could have been that the encoders were attached to the outer case of the induction machine, and doing this could atleast eliminate transverse vibration transmitted from the machine base.

Although there are lots of improvements needed, the set-up comes with some outstanding features

i. The excitation system is highly robust that uses cage induction machine and a frequency converter

ii. Frequency converter can be tuned for any value of peak torque at any frequency upto the rated condition of the small induction machine

iii. Once the set-up is ready the measurements can be done much faster

iv. One of the possible demerits is its limited use outside laboratory environment and quite expensive due to frequency converter.

References

[1] Harnefors, L., "Control of Variable Speed Drives," *Lecture Notes.* Department of Electronics, Malardalen University, Vasteras, Sweden, Sept. 11, 2003.

[2] Szenasi, Fred R. and Wachel, J. C., "Analysis of torsional vibrations in rotating machinery," *Proceedings of the Turbomachinery Symposium.* Vol. 22. Gas Turbine Laboratories, Department of Mechanical Engineering, Texas A & M University, pp. 127–151, 1993.

[3] Ehrich, F. F., *Handbook of Rotor Dynamics.* Malabar, Florida: Krieger, 1999, pp. 1.118–1.146.

[4] Ling Xiang, Shudong Li and Wei Cui, "Measurement and analysis of torsional vibration signal for rotating shaft system," in *Fuzzy Systems and Knowledge Discovery (FSKD), 9th International Conference*, 2012, pp. 1851–1854.

[5] Corbo, M. A., and Malanoski, S. B., "Practical design against torsional vibration," *Proceedings of the Twenty-Fifth Turbomachinery Symposium*, 1996, pp. 189–222.

[6] T. Holopainen, J. Niiranen, P. Jörg, and D. Andreo, "Electric Motors and Drives in Torsional Vibration Analysis and Design," *Proceedings of Forty-Second Turbomachinery Symposium*, Huston, Texas, Oct. 1–3, 2013.

[7] Jay P. Conniff and William F. Walker, Torin Corporation, "Apparatus for Fatigue Testing," U.S. Patent No.3, 495, 447, 1970.

[8] G. S. Zobrist, T. A. Dunlap, and R. H. Russell, Zonic Corporation, "Torsional Exciter for a Rotating Structure," U.S. Patent No.4,283,957, 1981.

[9] S. J. Drew, and B. J. Stone, "Torsional (rotational) vibration: excitation of small rotating machines," *Journal of sound and vibration* 201.4, pp. 437–463, 1997.

[10] S. J. Drew, D. C. Hesterman and B. J. Stone, "The torsional excitation of variable inertia effects in a reciprocating engine," *Mechanical Systems and Signal Processing,* vol. 13, pp. 125–144, 1, 1999.

[11] Sihler, C., "A novel torsional exciter for modal vibration testing of large rotating machinery," *Mechanical Systems and Signal Processing*, 20(7), pp. 1725–1740, 2006.

[12] Leong, J. H., Zhu, Z. Q., "A Novel Torsional Excitation Scheme for Determining Mechanical Transfer Function and Natural Frequencies of Circumferential Vibration in PM Brushless Machine Drives," *IEEE Transactions on Magnetics*, vol.47, no.10, pp. 4195–4198, Oct. 2011.

[13] Arkkio, A., "S–17.3050 Special Course in Electromechanics," *Lecture Notes.* Department of Electrical Engineering and Automation, Aalto University, Espoo, Finland, Sept. 9, 2013.

[14] Pal K. Kovacs, "Induction Motors," in *Transient phenomena in Electrical Machines*, Elsevier, 1984, pp. 30–134.

[15] Sheppard, D. J., "Torsional vibration resulting from adjustable-frequency AC drives," *IEEE Transactions on Industry Applications*, vol.24, no.5, pp. 812–817, Sep/Oct 1988.

[16] William T. Thomson and Marie D. Dahleh, "Harmonically Excited Vibration," in *Theory of Vibration with Applications*, Prentice Hall, 1998, pp. 49–75.

[17] Repo A.-K., Rasilo P. and Arkkio A., "Dynamic electromagnetic torque model and parameter estimation for a deep-bar induction machine," *IET Electric Power Applications* 2 (2008) 3, pp. 183–192.

A System Matrix

$$
A = \begin{bmatrix}
-\frac{R_{s1}}{L_{s1}'} & \omega_k & K_{r1}\frac{R_{s1}}{L_{s1}'} & 0 & 0 \\
-\omega_k & -\frac{R_{s1}}{L_{s1}'} & 0 & K_{r1}\frac{R_{s1}}{L_{s1}'} & 0 \\
K_{s1}\frac{R_{r1}}{L_{r1}'} & 0 & -\frac{R_{r1}}{L_{r1}'} & -(\omega_k-\omega_{01}) & 0 \\
0 & K_{s1}\frac{R_{r1}}{L_{r1}'} & -(\omega_k-\omega_{01}) & -\frac{R_{r1}}{L_{r1}'} & 0 \\
0 & 0 & 0 & 0 & -\frac{R_{s2}}{L_{s2}'} \\
0 & 0 & 0 & 0 & -\omega_k \\
0 & 0 & 0 & 0 & K_{s2}\frac{R_{r2}}{L_{r2}'} \\
0 & 0 & 0 & 0 & 0 \\
-M_1\psi_{ry0,1} & M_1\psi_{rx0,1} & M_1\psi_{sy0,1} & -M_1\psi_{sx0,1} & -M_2\psi_{ry0,2} \\
0 & 0 & 0 & 0 & 0 \\
-\frac{M_1}{J_1}\psi_{ry0,1} & \frac{M_1}{J_1}\psi_{rx0,1} & \frac{M_1}{J_1}\psi_{sy0,1} & -\frac{M_1}{J_1}\psi_{sx0,1} & \frac{M_2}{J_2}\psi_{ry0,2} \\
0 & 0 & 0 & 0 & 0
\end{bmatrix}
$$

$$
\begin{bmatrix}
0 & 0 & 0 & 0 & 0 & 0 & 0 \\
0 & 0 & 0 & 0 & 0 & 0 & 0 \\
0 & 0 & 0 & -\psi_{ry0,1} & 0 & -\frac{J_\mu}{J_1}\psi_{ry0,1} & 0 \\
0 & 0 & 0 & \psi_{rx0,1} & 0 & \frac{J_\mu}{J_1}\psi_{rx0,1} & 0 \\
-\omega_k & K_{r2}\frac{R_{s2}}{L_{s2}'} & 0 & 0 & 0 & 0 & 0 \\
-\frac{R_{s2}}{L_{s2}'} & 0 & K_{r2}\frac{R_{s2}}{L_{s2}'} & 0 & 0 & 0 & 0 \\
-\frac{R_{s2}}{L_{s2}'} & \frac{R_{r2}}{L_{r2}'} & (\omega_k-\omega_{02}) & \psi_{rx0,2} & 0 & \frac{J_\mu}{J_2}\psi_{rx0,2} & 0 \\
K_{s2}\frac{R_{r2}}{L_{r2}'} & -(\omega_k-\omega_{02}) & -\frac{R_{r2}}{L_{r2}'} & \psi_{rx0,2} & 0 & -\frac{J_\mu}{J_2}\psi_{rx0,2} & 0 \\
M_2\psi_{rx0,2} & M_2\psi_{sy0,2} & -M_2\psi_{sx0,2} & 0 & 0 & 0 & 0 \\
0 & 0 & 0 & 1 & 0 & 0 & 0 \\
\frac{M_2}{J_2}\psi_{rx0,2} & \frac{M_2}{J_2}\psi_{sy0,2} & -\frac{M_2}{J_2}\psi_{sx0,2} & 0 & 0 & 0 & 0 \\
0 & 0 & 0 & 0 & 0 & 1 & 0
\end{bmatrix}
$$

$$B = \begin{bmatrix} 1 & 0 & 0 & 0 & 0 & 0 & 0 & 0 & 0 & 0 & 0 & 0 \\ 0 & 1 & 0 & 0 & 0 & 0 & 0 & 0 & 0 & 0 & 0 & 0 \\ 0 & 0 & 1 & 0 & 0 & 0 & 0 & 0 & 0 & 0 & 0 & 0 \\ 0 & 0 & 0 & -1 & 0 & 0 & 0 & 0 & 0 & 0 & 0 & 0 \\ 0 & 0 & 0 & 0 & 1 & 0 & 0 & 0 & 0 & 0 & 0 & 0 \\ 0 & 0 & 0 & 0 & 0 & 1 & 0 & 0 & 0 & 0 & 0 & 0 \\ 0 & 0 & 0 & 0 & 0 & 0 & 1 & 0 & 0 & 0 & 0 & 0 \\ 0 & 0 & 0 & 0 & 0 & 0 & 0 & -1 & 0 & 0 & 0 & 0 \\ 0 & 0 & 0 & 0 & 0 & 0 & 0 & 0 & 1 & 0 & 0 & 0 \\ 0 & 0 & 0 & 0 & 0 & 0 & 0 & 0 & 0 & 0 & 0 & 0 \\ 0 & 0 & 0 & 0 & 0 & 0 & 0 & 0 & 0 & 0 & 1 & 0 \\ 0 & 0 & 0 & 0 & 0 & 0 & 0 & 0 & 0 & 0 & 0 & 0 \end{bmatrix}$$

Table A.1: Parameters of 37 kW cage-induction machine at no load condition

Parameter	**Value**
ψ_{sx0}	0.9856 Wb-t
ψ_{sy0}	0.0098 Wb-t
ψ_{rx0}	0.9588 Wb-t
ψ_{ry0}	0.0095 Wb-t
$L_{\mathrm{s}}{}'$	0.0023 H
$L_{\mathrm{r}}{}'$	0.0024 H
K_{s}	0.9697
K_{r}	0.9398
ω_{k}	314.1593 rad/sec
ω_0	314.1593 rad/sec

B Experimental Set-up

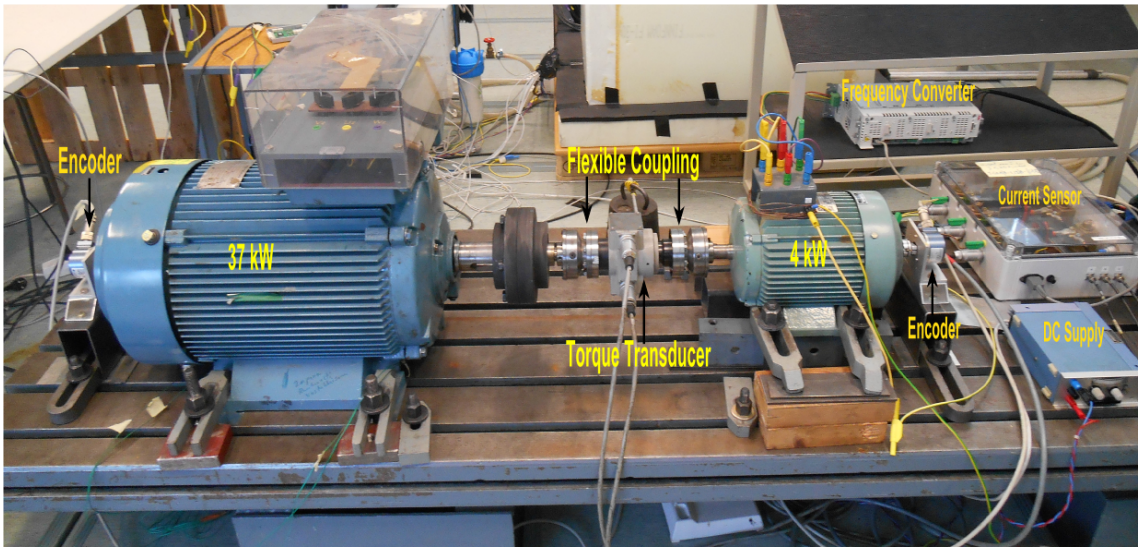

Figure B.1: Experimental set-up for torsion excitation

Figure B.2: Data logger unit